Invariant Epidemic Transient Decay From Radically Different Forms of Seasonal Forcing

Invariant Epidemic Transient Decay From Radically Different Forms of Seasonal Forcing

By Emma Coates, B.Sc.

A Thesis Submitted to the School of Graduate Studies in the Partial Fulfillment of the Requirements for the Degree Master of Science

Master of Science, Mathematics (2025)
Department of Mathematics & Statistics
McMaster University
Hamilton, Ontario, Canada

Title: Invariant Epidemic Transient Decay From Radically Different Forms of Seasonal Forcing
Author: Emma COATES, B.Sc.
Supervisor: Dr. David EARN
Number of pages: vii, 43

Abstract

This thesis begins by analyzing whooping cough dynamics in London from 1664 to 1950 in chapter 2. We use a historical whooping cough mortality time-series from the London Bills of Mortality and the Registrar General's Weekly Returns, in which a spectral analysis of the time-series reveals annual, biennial, triennial, and even quadrennial epidemic cycles. We originally sought to model and explain these transitions in the frequency structure of the whooping cough mortality data using the sinusoidally forced Susceptible-Infectious-Recovered (SIR) model [KM91]. The method of transition analysis previously used on historical disease-induced mortality time-series, including measles and smallpox [HE15, Kry11], relies on the existence of a period-doubling bifurcation in the basic reproduction number. Our analysis using this method on whooping cough, however, reveals the existence of only an annual attractor for relevant values of the basic reproduction number and amplitudes of forcing. Furthermore, the lack of bifurcations in relevant parameter spaces of our model for whooping cough led us to investigate the transient dynamics.

We explore the transient dynamics of the seasonally forced SIR model in chapter 3. Conveniently, we discover the transient periods of the associated annual attractor have potential to explain the transitions seen in the frequency structure of the whooping cough mortality data. We additionally consider a family of forcing functions when analyzing the transient dynamics. Prior to this work, it was unknown if the transient dynamics of the seasonally forced SIR model were invariant to the shape of seasonal forcing. Papst & Earn showed that key bifurcations of the standard SIR model are invariant to the shape of seasonal forcing if the amplitude of forcing is appropriately adjusted [PE19]. Our results from chapter 3 expand upon Papst & Earn's findings. We discover invariance in the decay of transient periods of the associated annual attractor from radically different shapes of seasonal forcing with appropriately adjusted amplitudes of forcing.

Acknowledgements

I would first like to thank my supervisor, Dr. David Earn, for his academic mentorship and support throughout my time here at McMaster. David's patience and expertise has helped me nurture my confidence and independence as a researcher. I am beyond grateful to continue studying under David's supervision in the years to follow.

I would also like to extend a special thank you to Dr. Irena Papst. Irena gifted her time and expertise during the final stages of this thesis. I am very excited to continue learning from her during my PhD.

Thank you to Drs. Ben Bolker and Jonathan Dushoff for being on my examining committee and for providing thoughtful edits and suggestions on the draft of this thesis.

Thank you to current members of the MacTheobio group for the weekly engaging discussions, and thank you to past members whose work I have learned so much from and has shaped this thesis. Though I'm an admittedly quiet member of the group, listening to the expertise and insights each of you brings has began shaping the way I think about math biology.

I would also like to thank my mentors from my undergraduate days at the University of Utah. If not for the support and encouragement of Drs. Alex Beams, Fred Adler, Damon Toth, and Lindsay Keegan, I would likely have not pursued graduate school. Thank you for all the knowledge and excitement for math biology you gifted me.

I would like to thank my fellow graduate students, who have become friends, for their companionship and community. I have learned so much from you all.

Finally, I would like to thank my family, and especially my partner Illya, for their love and support. Your encouragement and belief in me carried me through this mini-chapter in my graduate career.

Contents

List of Figures

List of Tables

Chapter 1

Introduction

Mathematical modelling is an exceptionally powerful tool in the study of infectious disease spread, both in understanding the underlying dynamics of how a disease spreads and in predicting these dynamics [Ear09, AM91]. In particular, mechanistic modelling has been extensively used for explanatory and inferential purposes when studying infectious disease dynamics [Ear09, AM91]. Mechanistic modelling investigates disease dynamics by making assumptions about how a disease spreads through a population, often over-simplifying the biological complexity of disease spread. These assumptions, however, give rise to flexible models that yield impactful, mathematical insight into disease dynamics. The frequency structure of recurrent epidemics varies over long time scales as external factors temporally affect epidemics, such as differing birth rates. Mechanistic modelling offers explanations and predictions of these frequency changes in historical incidence patterns of infectious diseases. Studying and understanding these frequency changes and their explanatory variables can allow for predictions of the timing of such transitions. Consequently, this is helpful in predicting ongoing epidemics and in improving public health strategies for disease control and eradication.

One of the more widely used mechanistic models is the standard Susceptible-Infectious-Recovered (SIR) model [KM91]. This model is popular among many infectious disease researchers as its simplicity allows for convenient and useful mathematical analyses and insights [Ear09]. The SIR model can additionally be seasonally forced, in various ways, but most often through the transmission rate, reflecting dynamics of recurrent epidemics. Additionally, the shape of seasonal forcing used in such models vary, although, sinusoidal forcing is more convenient to work with.

Our main goal in this thesis was originally to analyze and model whooping cough dynamics in London, U.K. from the mid-17th century until the mid-20th century using a historical whooping cough mortality

time-series. Whooping cough exhibits recurrent epidemics, as well as a changing frequency structure over the historical time-series. In chapter 2 we use the method of transition analysis (developed by Earn [ERBG00]) on the sinusoidally forced SIR model. The method of transition analysis used in this thesis provides a way to predict temporal transitions in epidemic cycles in incidence or mortality data by relating any seasonal forcing function to sinusoidal forcing. Papst & Earn [PE19] showed that key bifurcations in the seasonally forced SIR model are invariant to the shape of seasonal forcing if the amplitude of forcing is appropriately adjusted. This invariance allows the use of a transition anlaysis by matching period-doubling bifurcations in the sinusoidally forced SIR model with that of the SIR model forced with observed seasonal patterns. However, the analysis on the sinusoidally forced SIR model for relevant whooping cough parameters revealed only an annual cycle (i.e., there are no key bifurcations for relevant parameters), failing to address the changing frequency structure observed in the historical whooping cough mortality time-series. In response, we began investigating the transient dynamics of whooping cough. That is, we investigate the temporary dynamics of whooping cough between main epidemic cycles. In chapter 3, we examine the transient dynamics of whooping cough by looking at the transient periods of the associated annual attractor. While Papst & Earn [PE19] showed that key transitions in such frequency changes in the seasonally forced SIR model are invariant to the shape of seasonal forcing if the amplitude of forcing is appropriately adjusted, it is unknown if the transient dynamics are invariant to the shape of seasonal forcing. Furthermore, we consider a family of forcing functions when studying the transient dynamics of our model. This, perhaps not coincidentally, leads to the main finding of this thesis: The transient decay observed in the seasonally forced SIR model is invariant to radically different forms of seasonal forcing if the amplitude of forcing is appropriately adjusted. These findings are discussed in chapter 3. We first begin in chapter 2 by detailing the historical whooping cough mortality dataset, the importance of studying such a dataset, and the transition analysis and model used for studying whooping cough dynamics.

Chapter 2

Background and motivation: whooping cough dynamics in historical London

2.1 Introduction

Mechanistic modelling is considered a powerful tool in understanding the underlying dynamics of a disease and in predicting disease dynamics [Ear09, AM91]. Well-maintained data is often required to obtain useful insights from a mechanistic model, such as disease incidence, disease-induced mortality, and vital statistics, including birth and all-cause mortality [HE15, Ear09]. The London Bills of Mortality (LBoM) [Cre94] and the Registrar General's Weekly Returns (RGWRs) [RGW] together give meticulously kept accounts of weekly births, and weekly all-cause and whooping cough-induced mortality counts spanning from the mid-17th century until the mid-20th century in London, U.K.. Whooping cough exhibits recurrent epidemics, as well as a changing frequency structure over the historical time-series in London spanning 300 years. These complex transitions in the frequency structure and periodicities of infectious disease dynamics can result from external factors, such as changes in birth rates, and such transitions can be predicted using mechanistic models. In particular, the seasonally forced Susceptible-Infectious-Recovered (SIR) model [KM91] has been extensively used in the study of infectious disease dynamics [Ear09, ERBG00], and specifically in the study of the dynamics of historical childhood diseases [HE15, PE19, KE13, Ear09]. Our goal in this chapter is to identify the frequency structure of whooping cough-induced mortality in London during the 17th-20th centuries, and to model whooping cough dynamics using the standard sinusoidally forced SIR model. More specifically, we use the method of transition analysis introduced by Earn et al. [ERBG00] which can predict temporal transitions in epidemic cycles observed in incidence or mortality data.

2.2 Whooping Cough background

Whooping cough is a respiratory illness caused by the bacteria *Bordetella pertussis*, from which the clinical name of the disease "pertussis" is derived. *Bordetella* is a bacterium that adheres to the mucosal lining in the upper respiratory tract, causing inflamation in this lining while releasing toxins that further inflame the airways [AML24]. The infection causes repeated coughs followed by forceful inspiration, creating the characteristic 'whoop' sound, and causes symptoms similar to those of other infections of the upper respiratory tract. Serious complications occur mainly in infants, making pertussis particularly severe, and sometimes fatal, in this age group. An infection in infants is characterized by episodes of apnea, and other serious complications including pneumonia, the collapse of lungs, seizures, brain dysfunction, and cracked ribs [Can14]. Whooping cough is highly contagious and spread via aerosolized droplets produced by coughing [AML24].

The causative bacterium, *Bordetella pertussis*, was not isolated and identified until 1906. An effective vaccine was not developed until the 1940s and was first introduced into the routine childhood vaccination schedule in the United Kingdom in the 1950s [AML24]. Prior to the introduction of a vaccine, pertussis was a major cause of infant morbidity and mortality. English clinician Charles Creighton, on the topic of whooping cough mortality in London recorded by the RGWRs, writes "throughout the whole registration period, whooping-cough has kept its place steadily among the chief causes of infant mortality, neither decreasing nor increasing notably in the successive periods from 1837 to the present time [1894]. Its mortality has varied a good deal from year to year, owing to occasional great epidemic years such as 1866 and 1878; but on the mean annual average of decennial periods, it has varied little" [Cre94].

Infant mortality attributed to whooping cough was also recorded in other cities and countries beyond London during the 18th and 19th centuries. Swedish physician Nils Rosen von Rosenstein recorded an average of 2,712 deaths of children caused by pertussis in the years 1749-1764 in Sweden [Wes12]; the World Health Organization (WHO) estimated 160,700 deaths in children younger than 5 years worldwide in 2014 [WHO18]. Comparing the infant mortality of pertussis in Sweden in the 18th century and worldwide in 2014 with populations in those regions of approximately 1.8 million and 7.3 billion, respectively,

whooping cough was a significant cause of death among children in the 18th century.

Beyond infant morbidity and mortality, whooping cough epidemics peaked annually in London during the 19th and 20th centuries, as will be revealed in this study, with weekly mortality counts reaching beyond 200 individuals in the late 18th century. Inter-epidemic cycles of three and five years of the disease occurred during the 18th and 19th centuries as well [DC96]. Furthermore, the cyclic nature of the disease, both historically and currently, makes a seasonally forced mechanistic model an ideal tool for studying whooping cough. The historical dataset we study spans over 300 years and is well-maintained. Similar to the smallpox data studied by Krylova & Earn [KE20], the historical dataset we study spans over 300 years and is well-maintained. Such a dataset can allow us to understand the underlying periodicities and dynamics in the spread of whooping cough, which can then help us study and understand recent outbreaks of whooping cough. Although a widely-adopted vaccine has since been developed, whooping cough is still present worldwide, with cases rising in recent years since the SARS-CoV-2 pandemic [U.K]. Prior to the SARS-CoV-2 pandemic, the WHO estimated 24.1 million pertussis cases in 2014, with most cases occurring in low-income countries [WHO18]. With the understanding a historical dataset can give insights to the complex dynamics of a disease, we proceed by describing the historical data studied in the following section.

2.3 Description of the data

The data used in this study are digitized records of the LBoM [Cre94] and RGWRs [RGW]. These sources together give accounts of weekly births, and weekly all-cause and whooping cough mortality over an almost three-century long period from the mid-17th century to the mid-20th century in historical London, which is far smaller than the boundaries of modern London [Arc]. The Earn group digitized and cleaned both birth and death records from these sources, including weekly birth counts from the week of February 11, 1661 until December 27, 1930 and weekly all-cause and whooping cough deaths from the week of February 11, 1661 until December 12, 1950. The Earn group also harmonized this weekly mortality data, and we use this harmonized mortality dataset in our analyses. Note these digitized data sources are not yet published. The LBoM accounted for weekly births and deaths from the years 1661 to 1841. The RGWRs

for London had been recording births and deaths since 1837, however, records from RGWRs found in the the Cambridge University Library, the British Library, and the Wellcome Library don't begin until 1842 [KE20]. Consequently, birth and mortality data in this study starting from 1842 is sourced from the RGWRs.

While disease-related mortality is not what we aim to model, disease-specific mortality data can be used as a proxy for disease incidence. We additionally normalize the whooping cough mortality data by the trend of all-cause deaths in attempts to overcome the limitations of using mortality data to model the the incidence of whooping cough. Details of this normalization are described in section 2.3.2.

Vital statistics (i.e., births and natural deaths) impact the size of the population susceptible to contracting an infection, affecting the transmission dynamics of the infection. Accounting for births also allows us to estimate the *per-capita susceptible recruitment rate* (see eq. (2.3)), which is the rate at which individuals are "recruited", or born in this case, into the population that is susceptible to contracting the disease.

2.3.1 London Bills of Mortality and the transition to the Registrar General's Weekly Returns

The LBoM began more regularly reporting weekly Anglican baptisms and burials in 1604, however, it wasn't until 1661 that these records were reported without long gaps. It wasn't until October 18, 1664 that *weekly* baptism and burial records were reported consistently [KE20]. The LBoM presents various sampling deficiencies that were eventually addressed and corrected when the Registrar General began collecting vital statistics. Only burials of Anglican individuals were accounted for under the LBoM, and the LBoM fails to reflect the expansion of London's boundaries due to population growth from the years 1661 to 1841. It additionally fails to account for those buried outside city boundaries. Various other inconsistencies entered these records including impoverished Londoners being buried in non-Anglican grounds, and therefore unaccounted in the LBoM, and missing or inaccurate Parish returns with the rapid growth of London's population near the end of the 18th century [KE20]. The Registrar General's Office was created in 1836 [KE20] and by 1842 the RGWRs provided comprehensive and more accurate records of births and deaths than the LBoM. These records account for all deaths and all sectors of the population

(i.e., not just Anglican burials). As previously mentioned, the data in this study from beginning in 1842 and forward is sourced from the RGWRs.

As a result of the consistent weekly reports of baptisms and burials beginning in 1664 from the LBoM, we use that year as the starting date for the datasets. Consistent weekly birth data are digitized up to 1930. Weekly birth data estimates from the years 1931 to 1950 that have not been digitized are taken from Pyke's Master's project [Pyk19]. Pyke estimates these missing data by determining the average proportion of annual births in London compared to annual births in England and Wales from the years 1920 to 1930. This proportion is assumed to be constant after 1930. The product of this proportion and annual births in England and Wales for each year after 1930 is then divided by the number of weeks in each year to give the weekly estimate of births in London from the years 1931 to 1950. Pyke sourced the annual population estimates for London from the LBoM, and annual population estimates for England and Wales are sourced from UK census data [Dep13, Dat15, Pyk19]. There are additionally missing birth counts for a few years following the switch from the LBoM to the RGWRs, and these missing counts are estimated using linear interpolation by Pyke [Pyk19]. These data can be visualized in fig. 2.1.

2.3.2 Normalization

We want to normalize the weekly whooping-cough deaths to more accurately capture the burden and incidence of the disease over the time-series. The population size of London changed dramatically with the growing city boundaries over the three-centuries for which whooping cough deaths were reported. Additionally, the sampling deficiencies from the LBoM result in less complete, and under-reported, mortality data for whooping cough. These sampling deficiencies presumably affect deaths from all causes similarly, so rather than normalizing the whooping cough mortality time-series by London's estimated population size over three-centuries, we normalize the weekly whooping cough deaths by the trend of weekly all-cause mortality (ACM). This method aims to obtain a consistent normalization of weekly whooping cough deaths, and was used by Krylova & Earn when examining patterns of smallpox mortality reported from both the LBoM and the RGWRs in London over the same three centuries [Kry11, KE20]. Similarly to Krylova & Earn, the trend in the ACM is calculated using Empirical mode Decomposition (EMD). EMD is designed to identify trends in nonlinear and highly nonstationary time-series [KO09, Kry11, KE20], such

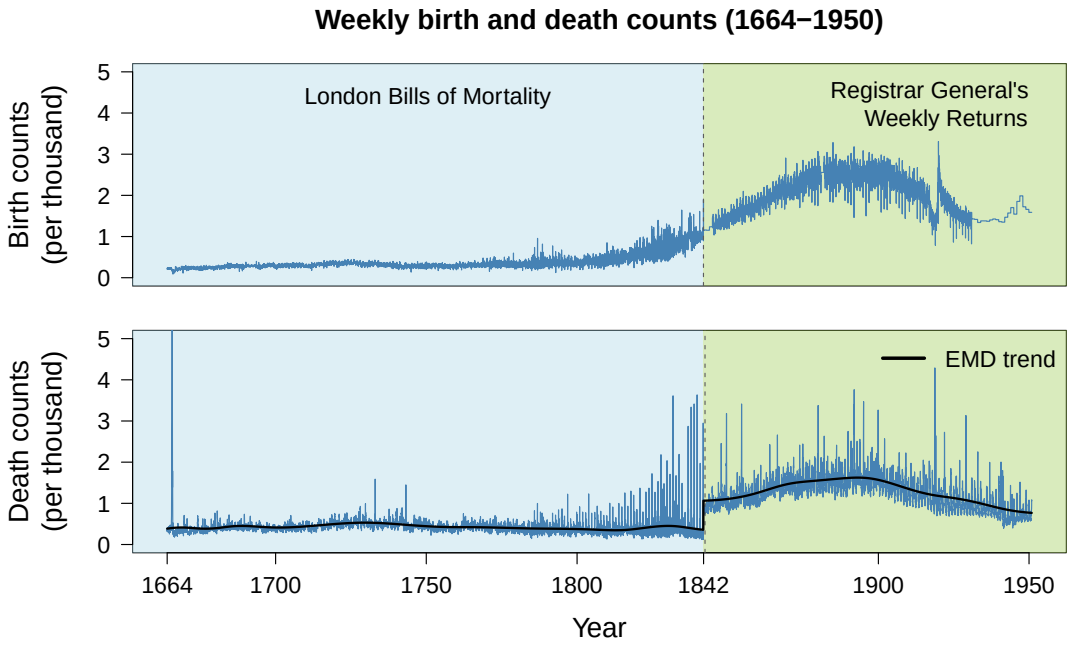

Figure 2.1: Weekly births and deaths (all-cause) in London, England from 1664 to 1950 collected by LBoM and RGWRs. In each panel, the distinction between data recorded from LBoM and RGWRs is emphasized by shading; the blue-shaded portion of the figures identify dates prior to 1842, in which data is taken from LBoM. The green-shaded portion of the figures identify dates after 1842, in which data is taken from the RGWRs. Weekly birth counts are presented in the first panel. Weekly birth data for the year 1842, immediately following the switch from LBoM to RGWRs, is missing in the digitized data and was estimated using linear interpolation. The weekly birth data after year 1930 was estimated as described above. Weekly all-cause mortality is presented in the second panel, where the first peak in 1665 caused by the Great Plague of London, resulting in 8,297 deaths per week [KE20], is cut off in the figure. The black curve along the all-cause mortality time-series is the trend of the signal estimated using Empirical Mode Decomposition [KO09, Kry11].

as the whooping cough and all-cause mortality time-series we have presented. This method decomposes a signal into several oscillatory components called Intrinsic Mode Functions (IMFs). IMFs are zero-mean oscillatory modes with well defined frequency ranges. The resulting IMFs represent different oscillations scales in the signal, with the first IMF encoding the highest-frequency oscillation and the subsequent IMFs encoding lower-frequency oscillations. After each IMF is extracted recursively starting from the original signal, the residual component is obtained by subtracting the sum of all the IMFs from the original signal; This residual component estimates the trend of the signal [KO09, Kry11, KE20]. Note that when EMD is

performed on any time-series in this study, it is done separately for the weekly data prior to 1842 and after 1842. This is primarily done to account for the sampling inconsistencies from the LBoM when estimating the trends in the time-series. The ACM time-series from 1664 to 1950, along with the trend of this signal computed using EMD, can be seen in fig. 2.1. The whooping cough mortality time-series, both the raw time-series and the normalized time-series, can be seen in fig. 2.2. The time-series reveal a cyclic nature in the pertussis-induced mortality; Visible peaks of mortality can be seen in fig. 2.2 from the 18th century until the end of the time-series (1950), but the length of the data makes visualizing the cycles of this mortality difficult. As the overall goal of this study is to understand the whooping cough dynamics, our goal in the following section is to identify the frequency structure of this time-series. Furthermore, we perform a spectral analysis on the whooping cough mortality time-series in order to identify predominant periodicities in the time-series, detailed in the following section.

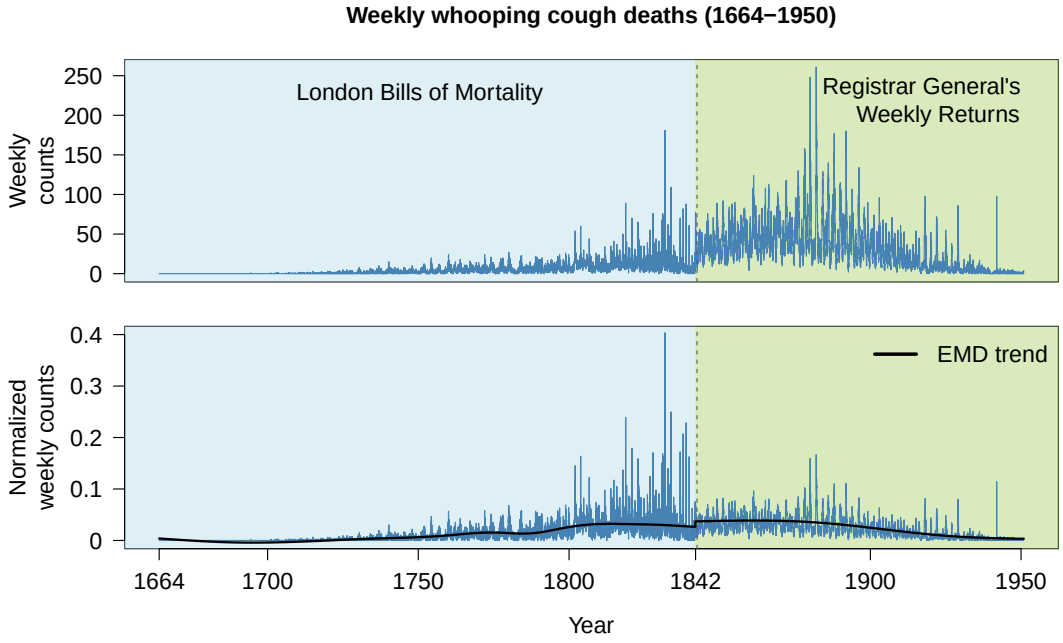

Figure 2.2: Weekly whooping cough (pertussis) mortality in London, England from 1664 to 1950 collected by LBoM and RGWRs. In each panel, the distinction between data recorded from LBoM and RGWRs is emphasized by shading, as in fig. 2.1. The raw mortality time-series is presented in top panel. The time-series normalized by the ACM trend (see fig. 2.1) is presented in the bottom panel. The solid black line in the bottom panel is the trend of the signal, estimated as in fig. 2.1.

2.4 Spectral analysis

We use spectral analysis to quantify periodicities in the whooping cough time-series and analyze how the frequency structure changes over time. Both a Fourier transform and a wavelet transform are used to identify these periodicities. Using both methods allows us to analyze the time-series locally and globally. The Fourier transform is the classical technique used to measure the frequency content of the entire time-series [Ear09], but it does not account for changes in the frequency structure over time. Wavelet analysis is a more sophisticated tool for examining how the frequency content of a time-series changes over time [Ear09, TC98]. Unlike traditional Fourier analysis, which assumes an observed time-series is stationary and provides only global frequency information, wavelet analysis performs a time-localized spectral decomposition, making it ideal for analyzing non-stationary signals. This method reveals how the frequency content changes over time without having to predefine separate temporal segments. Using both Fourier analysis and wavelet analysis is particularly important for the whooping cough mortality time-series we aim to analyze. The whooping cough mortality time-series is highly non-stationary, and external conditions over a three-century long period, such as differing birth rates, can affect the structure of the time-series across different segments. Prior to computing the transforms, the whooping cough mortality time-series is normalized, detrended using EMD, and square root transformed to minimize amplitude fluctuations without altering the underlying frequencies.

2.4.1 Classic power spectrum

We compute the standard power spectral density of the entire whooping cough mortality time-series, which corresponds to the classical Fourier analysis discussed above. We use the R function `spec.pgram()` [R C24], which calculates the spectral density with a fast Fourier Transform (FFT), with no taper and a standard modified Daniell smoother. The modified Daniell kernel with parameter m is a centered moving average which creates a smoothed value at time t by averaging all values between times $t - m$ and $t + m$, with the two endpoints in the averaging receiving half the weight that the interior points do [oS]. We use a smoother to filter out random noise in the signal and identify prominent spectral peaks with more clarity. The modified Daniell kernel used is convolved as well (`kernel = kernel(“modified.daniell”,`

`c(3,3))`). The Fourier spectral density of the normalized whooping cough time-series is plotted in fig. 2.3 as a function of period (in years). It highlights the existence of other major periods of 2, 2.5, and 3 years are highlighted as well. Longer period of 4 and 5 years are also detected, although, with less significant spectral density.

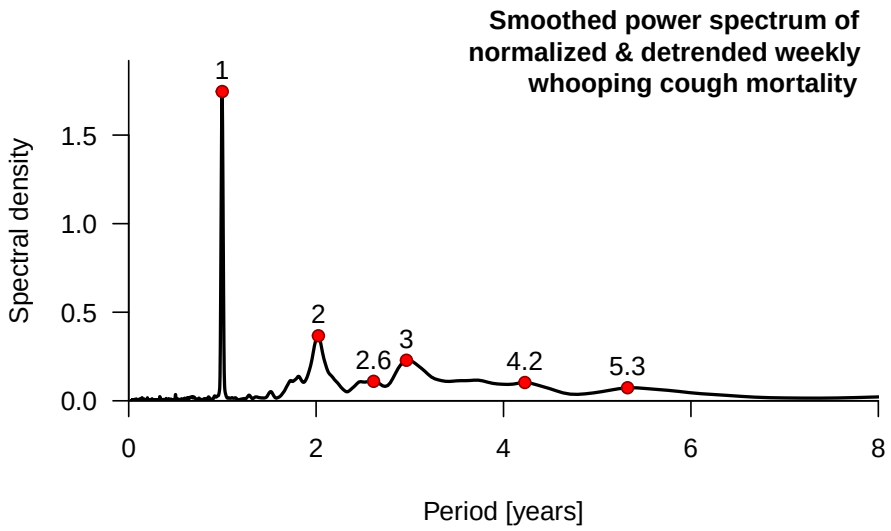

Figure 2.3: Standard power spectrum of the whooping cough mortality time-series. The time-series is normalized by the ACM trend (computed using Empirical Mode Decomposition (EMD) [KO09, KE20, Kry11]), detrended using EMD, and then square root transformed. The predominant period globally detected across the entire series is 1-year. The existence of other major periods of 2, 2.5, and 3 years are highlighted as well. Larger period of 4 and 5 years are also detected, although, with less significant spectral density.

2.4.2 Wavelet spectrum

The `analyze.wavelet()` function from the WaveletComp package in R [RS18] is used to obtain the continuous wavelet transform of the whooping cough time-series. The continuous wavelet transform is computed by convolving the time-series with scaled and shifted versions of a wavelet function [TC98]. A wavelet function, or analyzing wavelet, is a shape function with time and scale as parameters. The scale parameter of a wavelet function allows the function to be stretched or compressed to match low

or high-frequency structures within the time-series [TC98, KE20]. The Morlet wavelet is used as the wavelet function for the whooping cough mortality data. The convolution of the wavelet function (for a localized scale and time) and the time-series is computed, and if the wavelet correlates well with the signal at a specific time and scale, a larger value of the wavelet transform is recorded. If the wavelet does not correlate well with the signal at a specific time and scale, a smaller value is recorded for the wavelet transform. This method applied along the entire time-series and over a continuous range of a scale parameter decomposes the time-series into time and frequency domain [TC98, KE20]. This results in a two-dimensional figure, which is shown in fig. 2.4. Similar to the standard power spectrum, the wavelet transform reveals dominant periods of 1 year and between 2 years and 4 years. Again, the wavelet transform allows us to identify temporal patterns of the frequency structure of the whooping cough time-series. The predominant period in the whooping cough mortality time-series is 1-year for the majority of the time-series. More specifically, from the late 17th century to the early 20th century, there is an annual peak in mortality from whooping cough. We can thus assume there is an annual cycle in whooping incidence during those centuries. Significant periods between 2 and 4 years in whooping cough epidemic patterns are detected across the time-series as well. Prior to 1842, an annual period is also detected; however, multi-period patterns in the data have similar spectral power.

While both the classical Fourier analysis and the more sophisticated wavelet analysis reveal a dominant period observed in the mortality time-series of 1 year, the wavelet spectrum reveals transitions in frequencies of these epidemic cycles. Within the 95% confidence contour in fig. 2.4, epidemic peaks transition from annual to biennial (every two years), triennial (every three years), and quadrennial (every four years). We aim to understand and model these transitions in epidemic cycles with a seasonally forced mechanistic model. In particular, we use the standard Susceptible-Infectious-Recovered (SIR) model [KM91], as we describe in the following section.

2.5 The Susceptible-Infectious-Recovered model

We begin our analysis by introducing the standard Susceptible-Infectious-Recovered (SIR) model [KM91] with vital dynamics, which subdivides a population in compartments of susceptible, infectious, and re-

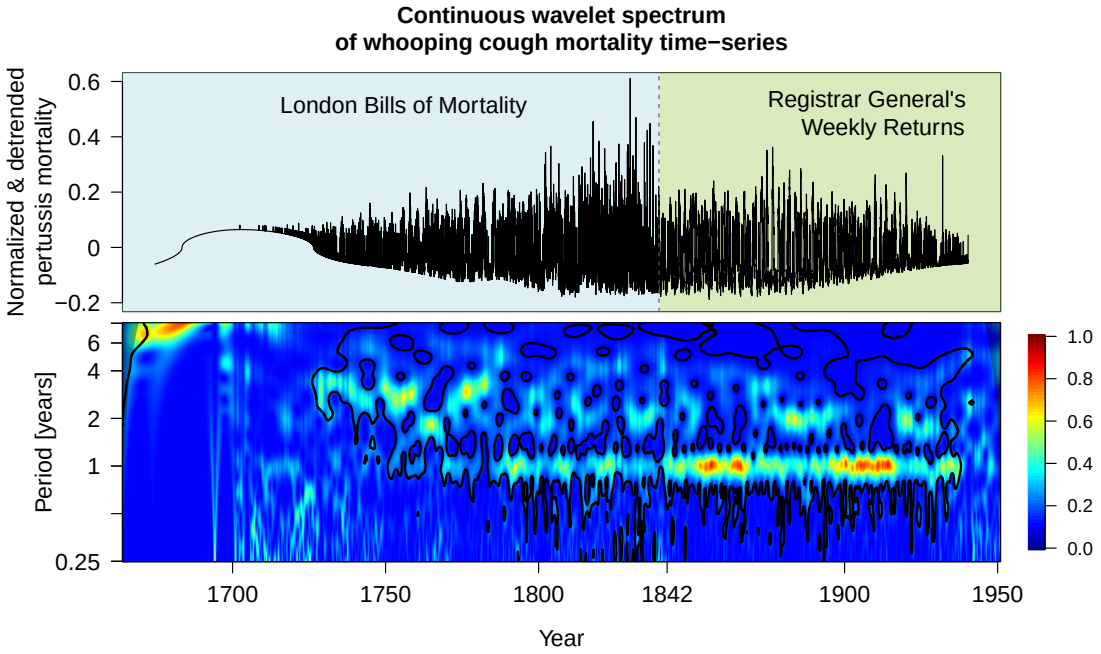

Figure 2.4: Continuous wavelet spectrum of the whooping cough mortality time-series. The time-series normalized by the ACM trend (computed using Empirical Mode Decomposition (EMD) [KO09, KE20, Kry11]), detrended using EMD, and then square root transformed is presented in the top panel. The continuous wavelet transform of this data is presented in the bottom panel. The thin black contour in the bottom panel is the 95% confidence interval, and the medium black contour is the cone of influence, in which regions have lower accuracy [TC98, RS18]. The predominant period in the whooping cough mortality time-series is 1-year for the majority of the time-series. More specifically, from the late 17th century to the early 20th century, there is an annual peak in mortality from whooping cough. We can thus assume there is an annual cycle in whooping incidence during those centuries. There is additionally points along the time-series where strong periods of 2 and 3 year cycles of mortality from whooping cough exist.

covered (immune) in regards to the disease. Written in terms of the host population that are susceptible, infectious, and recovered denoted by S, I, and R, respectively, the SIR model is given by [HE15]

$$\frac{dS}{dt} = \nu N_0 - \beta S I - \mu S, \tag{2.1a}$$

$$\frac{dI}{dt} = \beta S I - (\gamma + \mu) I, \tag{2.1b}$$

$$\frac{dR}{dt} = \gamma I - \mu R. \tag{2.1c}$$

Equations (2.1a, 2.1b) are independent of the state variable R, and thus the full dynamics of the system can be described in two dimensions while ignoring the third equation. The parameters are the rates of transmission (β) and recovery (γ), as well as the per capita rates of birth (ν) and death (μ) which model vital dynamics in the host population. We interpret the birth rate (ν) to be the per capita susceptible recruitment rate, and the per capita death rate (μ) to represent deaths by natural causes exclusively. We assume disease-induced mortality is negligible. $T_{\text{inf}} = 1/\gamma$ gives the mean infectious period. N_0 refers to the population at a specified 'anchor time' t_0 [BE03, Ear09, ERBG00, HE15, KE13].

The basic reproduction number, $\mathcal{R}_0$, is the average number of secondary cases caused by a primary case in a wholly susceptible population [AM91, Ear09]. $\mathcal{R}_0$ is given by [KE13]

$$\mathcal{R}_0 = \frac{\nu N_0}{\mu} \frac{\beta}{\gamma + \mu}. \tag{2.2}$$

We assume that the susceptible recruitment rate ν changes slowly enough that $\mathcal{R}_0$ can be defined by (2.2) at a given time by treating ν as a constant [HE15]. Anderson and May estimated the basic reproduction number of whooping cough in 1950 to be 17 [AM91]. We use this estimate of $\mathcal{R}_0$ from the year 1950, and consequently choose our anchor time to be the year 1950.

2.5.1 Susceptible-Exposed-Infectious-Recovered

Recent work on childhood disease dynamics has been based on the SIR model rather than the Susceptible-Exposed-Infectious-Recovered (SEIR) model [HE15, KE20, PE19] despite most previous work using the SEIR model. The SEIR model includes an additional class (E) of exposed individuals from the host population that are infected but not yet infectious. Krylova & Earn [KE13] showed that bifurcation diagrams for the SIR model are nearly equivalent to those of the SEIR model if the mean generation time is taken to be the mean infectious period. The generation time, or the generation interval, is the time between the onset of infection of a primary case and the onset of secondary case [KE13]. The mean generation time for the SIR model is often taken to be the sum of the latent period (T_{lat}) and the mean infectious period (T_{inf}) [KE13, HE15, PE19]. We follow recent work [HE15, KE20, PE19] and use the SIR model (2.1) with the mean generation time ($T_{\text{lat}} + T_{\text{inf}}$) as the mean infectious period for our analysis.

2.5.2 Seasonality

Epidemic cycles are often undamped, including those of childhood diseases such as measles, mumps, rubella, and whooping cough. Generally, transmission rates of these childhood diseases vary seasonally with school terms [Ear09]. The transmission rate is the product of the contact rate among individuals and the probability of infection per infectious contact [Ear09], so we assume the transmission rate must vary seasonally for childhood diseases as the rate of contact of children rises during school terms. The most common approximation of this seasonality is to assume that β varies sinusoidally [Ear09, KE13, PE19, HE15]

$$\beta(t) = \beta_0 (1 + \alpha \cos(2\pi t)), \tag{2.3}$$

where β_0 is the mean transmission rate, α ($0 \leq \alpha \leq 1$) is the amplitude of forcing, and time t is measured in years. The SIR model is said to be seasonally forced with $\beta(t)$ as in (eq. (2.3)), where $\beta(t)$ has a period of 1 year. While the SIR model in general is an abstract model with no intrinsic reason to be seasonally forced via the transmission term with a period of 1 year, we take the period to be 1 year since we are modelling childhood diseases.

Variation in contact rates of children is not sinusoidal, but rather driven by school terms [Ear09]. The primary driver of seasonal forcing of childhood diseases is generally school terms [PE19, LY73]. This particular forcing has been modeled with what is called *term-time forcing* and is defined by Earn [Ear09] as follows [Ear09, PE19, Sch84, ERBG00],

$$\beta_{\text{tt}}(t) = \begin{cases} \beta_{\text{high}} & \text{school days,} \\ \beta_{\text{low}} & \text{other days,} \end{cases} \tag{2.4}$$

where the transmission rate is high on days when school is in session (β_{high}) and low otherwise (β_{low}), with $\beta_{\text{high}} > \beta_{\text{low}}$. If the proportion of days per year spent in school is p_{s}, then the average transmission rate becomes

$$\langle \beta \rangle = p_{\text{s}} \beta_{\text{high}} + \left(1 - p_{\text{s}}\right) \beta_{\text{low}}, \tag{2.5}$$

and we define the amplitude of seasonality to be

$$\alpha = \frac{1}{2}\frac{\beta_{\text{high}} - \beta_{\text{low}}}{\langle\beta\rangle}. \tag{2.6}$$

From eq. (2.5) and eq. (2.6), we can define the oscillation function to be

$$\text{osc}_{\text{tt}} = \begin{cases} 2\left(1 - p_{\text{s}}\right) & \text{school days,} \\ -2p_{\text{s}} & \text{other days,} \end{cases} \tag{2.7}$$

and rewrite eq. (2.4) in terms of parameters $\langle\beta\rangle$ and α

$$\beta_{\text{tt}} = \langle\beta\rangle\left(1 + \alpha\text{osc}_{\text{tt}}\right). \tag{2.8}$$

Term-time forcing can successfully account for observed childhood disease dynamics, namely measles [Ear09, ERBG00]. However, Papst & Earn showed that key bifurcations of the standard SIR model are invariant to the shape of seasonal forcing if the amplitude of forcing is appropriately adjusted [PE19]. These key bifurcations refer to period-doubling bifurcations in $\mathcal{R}_0$. Past work in estimating the amplitude of forcing for childhood diseases has relied on period-doubling bifurcation points in $\mathcal{R}_0$ [HE15]. Estimates of the seasonal forcing amplitude are obtained by matching the period-doubling bifurcation points that arise from the sinusoidally forced SIR model with that of the observed seasonal pattern from disease-incidence or mortality data. A series of bifurcation diagrams in $\mathcal{R}_0$ for different forcing amplitudes is constructed until one of the forcing amplitudes yields a bifurcation diagram for which the period-doubling bifurcation point occurs at the same value of $\mathcal{R}_0$ as in the bifurcation diagram made with the observed seasonal forcing pattern [PE19]. Furthermore, we proceed in our analysis with the *sinusoidally* forced the SIR model for convenience.

2.5.3 Effective reproduction number $\mathcal{R}_{0,\text{eff}}$

The *effective reproduction number* $\mathcal{R}_{0,\text{eff}}$ is the average number of secondary cases caused by a single primary cases in a host population comprised of *both* susceptible and non-susceptible individuals [HE15];

in other words, $\mathcal{R}_{0,\text{eff}}$ is analogous to $\mathcal{R}_0$ in population that is *not* wholly susceptible. We can thus estimate $\mathcal{R}_{0,\text{eff}}$ by altering $\mathcal{R}_0$ with factors of the susceptible recruitment rate ν. We define the susceptible recruitment rate as [HE15]

$$\nu(t) = \frac{B(t) - D_{\text{infant}}}{N_0}, \tag{2.9}$$

where $B(t)$ is the number of births at time t, D_{infant} is the number of infant mortalities at time t, and N_0 is the population at the chosen anchor time t_0. Infant mortalities are deducted in eq. (2.9) to account for reduction in new susceptibles [HE15]. Now we can define $\mathcal{R}_{0,\text{eff}}$ [HE15]

$$\mathcal{R}_{0,\text{eff}} = \frac{\nu(t)}{\nu_0}\mathcal{R}_0, \tag{2.10}$$

where ν_0 is the susceptible recruitment rate at the anchor time t_0. All estimates for relevant parameters in the model are summarized in table 2.1.

Parameter	**Interpretation**	**Estimate**	**Source**
Fixed			
γ^{-1}	Mean Infectious Period	22 days	[AM91]
μ	Natural Death Rate	0.02 yr^{-1}	[ERBG00]
N_0	Population in London at 1950	8,260,440	[ERBG00]
$\mathcal{R}_0$	Basic Reproduction Number in 1950	17	[AM91]
ν_0	Susceptible Recruitment Rate in 1950	0.00942 yr^{-1}	eq. (2.9)
Time-varying			
ν	Susceptible Recruitment Rate	0.0141 – 0.0009 yr^{-1}	eq. (2.9)
$\mathcal{R}_{0,\text{eff}}$	Effective Reproduction Number	2.506528 – 25.48721	eq. (2.10)
D_{infant}	Infant Deaths	0.0000078 – 0.00018 yr^{-1}	[MD86]

Table 2.1: Whooping cough parameter estimates

2.6 Method of transition analysis

The method of transition analysis deployed in this study (developed by Earn [ERBG00]) is a useful tool for predicting temporal transitions in epidemic cycles in observed incidence or mortality data. A transition

analysis examines both resonant and non-resonant periods in solutions to the seasonally forced SIR model and compares these periods with the frequency structures revealed from a spectral analysis of an observed incidence or mortality time-series. We proceed by examining the resonant periods of the sinusoidally forced SIR model.

2.6.1 Attractor and transient periods as functions of $\mathcal{R}_0$

The period of the attractor that is reached asymptotically and the period of the damped oscillations onto that attractor (transient period) can be extracted from solutions to the SIR model. The attractor period of the SIR model is always an integer multiple of the 1-year forcing period and can be inferred from bifurcation diagrams of solutions mapped onto a stroboscopic map [HE15]. It is convenient to map solutions of the periodically forced SIR model onto a stroboscopic map with a one-year strobing interval. The stroboscopic map discretely samples solutions once per forcing period, which will result in k points being returned for a k-period cycle. The output from the stroboscopic map is therefore convenient for identifying periods of the attractors. A linear perturbation analysis of a particular attractor yields the associated transient period, or the period of damped oscillations onto the associated attractor. The transient periods can be non-integer multiples of the 1-year forcing period and are given by [BE03]

$$T_k = \frac{2\pi k}{\left|\mathrm{Arg}(\lambda_k)\right|}, \tag{2.11}$$

where λ_k is the dominant (complex) eigenvalue of the associated stroboscopic map.

We follow Krylova & Earn [KE13], and Hempel & Earn [HE15], and take advantage of the relationship between susceptible recruitment (eq. (2.9)) and effective reproduction number (eq. (2.10)). This allows us to make predictions from the SIR model (eq. (2.1)) with $\mathcal{R}_0$ acting as the only relevant parameter. Furthermore, we make predictions considering only how periodicities of solutions vary as a function of the basic reproduction number $\mathcal{R}_0$ (eq. (2.2)), with all other parameters fixed, and assume the amplitude of seasonality can be taken to be constant through the observed time-series. We do so by numerically constructing one-parameter bifurcation diagrams in $\mathcal{R}_0$ using the standard open-source software XPPAUT [Erm02]. We follow the numerical process and method of the continuation of bifurcations outlined by

Krylova & Earn [Kry11] and Papst & Earn [PE19]. We constructed brute-force bifurcation diagrams (i.e., we did not use AUTO, and simply ran XPPAUT in batch mode to extract the data for the one-parameter bifurcation diagrams (see the supplemental materials from Papst & Earn's work [PE19])). The resulting bifurcation diagrams in $\mathcal{R}_0$ for small forcing amplitudes are shown in fig. 2.5. For forcing amplitudes of value 0.1 and smaller, only an annual attractor for the full range of chosen $\mathcal{R}_0$ values for the given set of parameter values (see table 2.1). Reasonable amplitudes of forcing for the sinusoidally forced SIR model in the context of childhood diseases are generally very small. For example, Earn et al. suggest a reasonable amplitude of forcing for measles modeled using a sinusoidally forced SIR model is around $\alpha = 0.08$, "most previous discussions of measles dynamics have assumed sinusoidal seasonal forcing with an amplitude of 0.28, which yields a chaotic attractor; this level of forcing is about three times higher than it should be" [ERBG00]. Furthermore, what we assume to be reasonable amplitudes of forcing for whooping cough yield only annual attractors. The original goal of this study was to analyze the transitions observed in the 300-year long whooping cough mortality time-series; however, in order to do so, we must have a method for estimating the forcing amplitude for the seasonally forced SIR model from the observed seasonal patterns. As mentioned in section 2.5.2, the method we aim to use for estimating the forcing amplitude involves constructing a series of bifurcation diagrams in $\mathcal{R}_0$ for different forcing amplitudes until one of these diagrams yields a bifurcation diagram for which the period-doubling bifurcation point occurs at the same value of $\mathcal{R}_0$ as in the bifurcation diagram made with the observed seasonal forcing pattern.

As the transition analysis of our model for whooping cough reveals only an annual resonant period for small forcing amplitudes, we are unable to estimate the forcing amplitude using previously employed techniques [KE13, HE15], and the transition analysis for the patterns observed in the whooping cough time-series remains incomplete. The frequency structure of the whooping cough mortality time-series studied in the spectral analysis reveals an annual cycle along with transitions to biennial, triennial, and quadrennial epidemic cycles that the resonant dynamics of our model do not explain.

Instead, this shortcoming incidentally leads to deeper investigations of the non-resonant periods of solutions to the SIR model. In particular, we attempt to study the transient dynamics of the associated annual attractor in order to explain the lack of transitions in the resonant period of the sinusoidally forced

model. We explore the decay in the non-resonant periods (associated with the annual resonant periods) as functions of $\mathcal{R}_0$ and compare these periods with the spectral analysis. We additionally explore the resulting invariance these non-resonant periods share with invariance in the key bifurcations discovered by Papst & Earn [PE19] from different forms of seasonal forcing in the following chapter (Chapter 3).

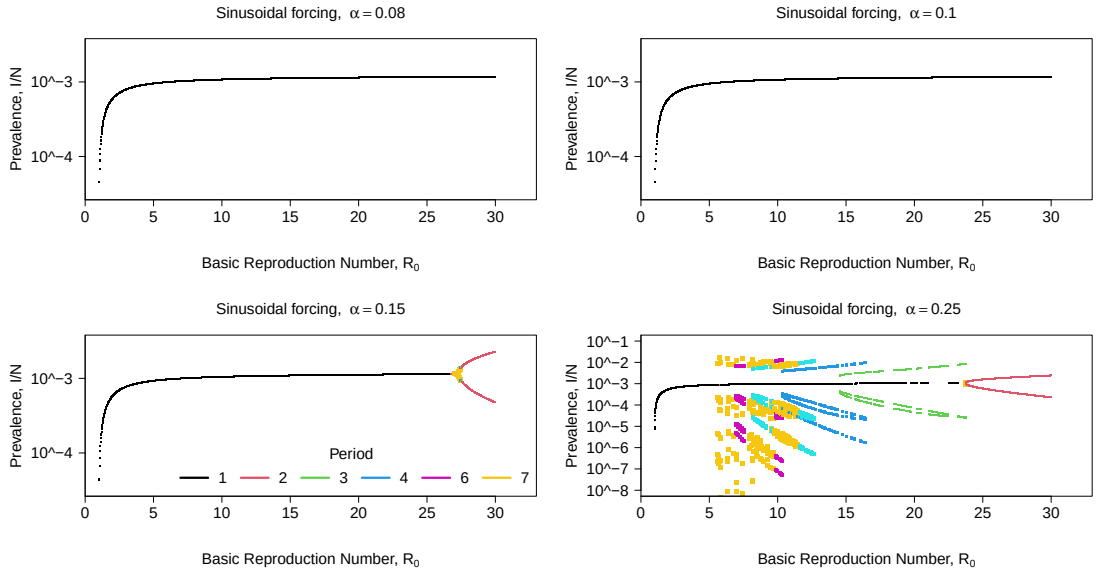

Figure 2.5: One-parameter bifurcation diagrams in $\mathcal{R}_0$ of the sinusoidally forced SIR model constructed with $\gamma^{-1} = 22$ days. Each bifurcation diagram is constructed with a particular amplitude of forcing, α, indicated in the titles. The bifurcation diagram in the first column, last row holds the legend indicating which period is associated with which color, that is relevant for all four diagrams. The bifurcation diagrams in the first row indicate for small α, there only exists a 1-year periodic orbit, or an annual attractor. As α increases, a stable period-two orbit is born. However, reasonable amplitudes of forcing for the sinusoidally forced SIR model in the context of childhood diseases are generally very small. For example, Earn et al. suggest a reasonable amplitude of forcing for measles modeled using a sinusoidally forced SIR model is around $\alpha = 0.08$ [ERBG00].

Chapter 3

Invariant epidemic transient decay from radically different forms of seasonal forcing

3.1 Introduction

The approach used by Papst & Earn [PE19] for the method of transition analysis proves to be problematic for whooping cough as there isn't a period-doubling bifurcation near relevant values of $\mathcal{R}_0$. Furthermore, Papst & Earn did not investigate the invariance of transient dynamics from different forms of seasonal forcing. Our goal is to investigate invariance of transient dynamics from different forms of seasonal forcing and determine whether transient dynamics associated with the annual attractor can be matched rather than matching the period doubling bifurcation. We proceed by introducing a family of forcing functions developed by Papst & Earn in order to explore the potential invariance from these different forms of seasonal forcing. We additionally consider the dynamics of the unforced SIR model, specifically the damped oscillations onto the equilibrium of solutions, as the straightforward analytical expression for the period of these oscillations can lend insight into the transient dynamics of the seasonally forced model. We additionally reference chapter 2, in which the resonant dynamics of the sinusoidally forced model fail to explain the transitions in epidemic cycles observed in the whooping cough mortality time-series. We then briefly discuss the potential the transient dynamics possess in explaining the epidemic transitions observed in whooping cough.

3.2 Family of forcing functions

While Papst & Earn showed that the key bifurcations of the seasonally forced SIR model are invariant to the shape of seasonal forcing with an appropriate adjustment of the amplitude of forcing [PE19], it is unknown if the transient dynamics of the SIR model share this invariance. In order to better understand how these transient dynamics depend on the pattern of seasonality in transmission, we consider different shapes of seasonal forcing. Namely, we incorporate a continuous family of forcing functions, which connects term-time (discussed and defined in section 2.5.2) and sinusoidal forcing, developed by Papst & Earn [PE19] into the analysis. The family is parameterized with a shape parameter p, such that the forcing follows the school term schedule when $p = -1$, is square and symmetric when $p = 0$, and is sinusoidal when $p = 1$. Papst & Earn define the family of forcing functions as follows.

The shape functions for term-time forcing to square wave forcing is given by

$$\text{TTtoSquare}\,(t, p) = \begin{cases} 1 & \text{school days,} \\ -1 & \text{other days,} \end{cases} \tag{3.1}$$

where school days and non-school days get scaled linearly with p. The shape function for square wave forcing to sinusoidal forcing is given by

$$\text{SquaretoCos}\,(t, p) = \text{sign}\big(\cos(2\pi t)\big)\Big|\cos(2\pi t)\Big|^{p}, \tag{3.2}$$

where $\text{sign}(x)$ is the signum function, which evaluates to 1 if $x > 0$, -1 if $x < 0$, and 0 otherwise. Both functions are pieced together into one shape function to give

$$s\,(t, p) = \begin{cases} \text{TTtoSquare}\,(t, p) & -1 \leq p \leq 0, \\ \text{SquaretoCos}\,(t, p) & 0 \leq p \leq 1. \end{cases} \tag{3.3}$$

The family of forcing functions is then defined as

$$\mathrm{osc}_p(t) = \begin{cases} s(t,p) + 2\left(1 - p_\mathrm{s}\right) & -1 \le p \le 0, \\ s(t,p) & 0 \le p \le 1, \end{cases} \tag{3.4}$$

where

$$2\left(1 - p_\mathrm{s}\right) = \int_0^1 \mathrm{osc}_{p<0}(t)\, dt, \tag{3.5}$$

which is the average value of a single period $\mathrm{osc}_{p<0}$ before being shifted. This is done to ensure the forcing functions used in the SIR model have an average value of zero. Finally, the SIR model is forced through the transmission rate β with this family of forcing functions as follows:

$$\beta_p(t) = \langle\beta\rangle\left(1 + \alpha \mathrm{osc}_p(t)\right), \tag{3.6}$$

where the functions is vertically scaled with the amplitude of seasonality α and vertically shifted by the mean transmission rate $\langle\beta\rangle$. Members of this family of forcing functions are given in fig. 3.1.

3.3 Period of damped oscillations of the unforced SIR model as a function of $\mathcal{R}_0$

We begin our analysis by first considering the damped oscillations of solutions to the *unforced* SIR model and their associated periods. While we are primarily interested in understanding the dynamics that arise from seasonal patterns in epidemics, and therefore interested in examining the dynamics of the seasonally forced SIR model, understanding behavior in the unforced model can lead to insights of behavior in the forced model. It is straightforward to analytically derive the period of the damped oscillations onto the equilibrium of the solution to the unforced model. This analytical convenience has the potential to reveal insights to the forced model and its transient periods. We proceed by deriving the period of these damped oscillations, following the derivation that He & Earn outline [HE07] with some slight adjustments.

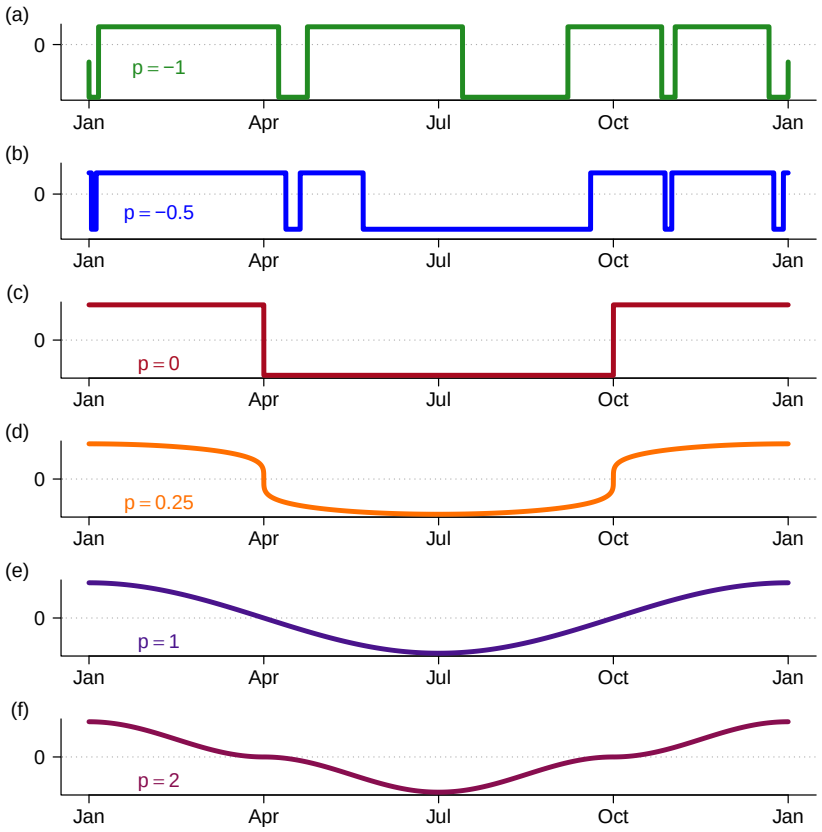

Figure 3.1: A recreated figure from Papst & Earn ([PE19], Figure 2) detailing several members of the family of forcing functions, $\mathrm{osc}_p(t)$, described in Section 3.2. (a) $p = -1$ (term-time forcing), (b) $p = -0.5$, (c) $p = 0$ (square wave forcing), (d) $p = 0.25$, (e) $p = 1$ (sinusoidal forcing), (f) $p = 2$.

For convenience, we introduce a dimensionless parameter, defined by Parsons & Earn [PE24],

$$\varepsilon = \frac{\mu}{\gamma + \mu} \tag{3.7}$$

which expresses the mean infectious period in units of the mean host lifetime [PE24].

The unforced SIR model (eq. (2.1)) has at least one and at most two equilibria; for any combination of parameter values, there exists the disease free equilibrium (DFE, $(S, I) = (1, 0)$), which is globally asymptotically stable for $\mathcal{R}_0 \leq 1$ and unstable if $\mathcal{R}_0 > 1$ [Het76]. If $\mathcal{R}_0 > 1$, then there exists a globally

asymptotically stable endemic equilibrium (EE),

$$S^* = \frac{\nu}{\mu}\frac{1}{\mathcal{R}_0} \tag{3.8a}$$

$$I^* = \frac{\nu}{\mu}\varepsilon\left(1 - \frac{1}{\mathcal{R}_0}\right) \tag{3.8b}$$

Since we are interested in the dynamics for $\mathcal{R}_0 > 1$, we examine the local stability of the endemic equilibrium and later extend this local stability analysis to the seasonally forced SIR model.

Letting $S = \dot{S} - \Delta S$ and $I = \dot{I} - \Delta I$, we linearize eq. (2.1a)-eq. (2.1b) about the endemic equilibrium (eq. (3.8)) and ignore quadratic terms (i.e., $\Delta S \Delta I$),

$$\begin{pmatrix} \Delta\dot{S} \\ \Delta\dot{I} \end{pmatrix} = \begin{pmatrix} -\mu\mathcal{R}_0 & -\mu\varepsilon \\ \mu\left(\mathcal{R}_0 - 1\right) & 0 \end{pmatrix}\begin{pmatrix} \Delta S \\ \Delta I \end{pmatrix}. \tag{3.9}$$

The eigenvalues of the Jacobian above are

$$\lambda_{\pm} = r \pm i\omega \tag{3.10}$$

with

$$r = -\frac{\mu\mathcal{R}_0}{2}, \tag{3.11}$$

and

$$\omega = \mu\sqrt{\frac{1}{\varepsilon}\left(\mathcal{R}_0 - 1\right) - \left(\frac{\mathcal{R}_0}{2}\right)^2}. \tag{3.12}$$

The solutions to eq. (2.1) when $\mathcal{R}_0 > 1$ will approach the endemic equilibrium via damped oscillations if and only if

$$\varepsilon < \varepsilon^* = \frac{4\left(\mathcal{R}_0 - 1\right)}{\mathcal{R}_0^2}. \tag{3.13}$$

For typical childhood infectious diseases, $\varepsilon < 10^{-3}$ and $\mathcal{R}_0 \ll 10^2$ [HE07]. Assuming $\nu \approx \mu$, $\varepsilon \ll 0.04 < \varepsilon^*$, so we can assume that inequality (3.13) will be satisfied for our purposes, resulting in damped oscillations

onto the endemic equilibrium. The natural frequency of these oscillations is ω and their period is given by

$$T = \frac{2\pi}{\omega} = 2\pi \left[\frac{1}{\mu} \left(\frac{1}{\varepsilon}(\mathcal{R}_0 - 1) - \left(\frac{\mathcal{R}_0}{2} \right)^2 \right)^{-1/2} \right]. \tag{3.14}$$

3.4 Transient period as a function of $\mathcal{R}_0$ for radically different forms of seasonal forcing

We now shift our attention to computing the periods of the damped oscillations onto the annual attractor of the seasonally forced SIR model, while considering different forms of seasonal forcing using the family of forcing functions defined in Section 3.2. The transient periods associated with the annual attractor are given by

$$T_1 = \frac{2\pi}{\left|\text{Arg}(\lambda_1)\right|}, \tag{3.15}$$

where λ_1 is the dominant (complex) eigenvalue of the associated stroboscopic map evaluated at the annual periodic orbit, or the characteristic (Floquet) multipliers of that periodic orbit [Str18]. Generally, Floquet multipliers can only be found via numerical integration [Str18]. Similarly to the one parameter bifurcation diagrams constructed in chapter 2, we follow the numerical process of the continuation of bifurcations outlined by Papst & Earn in the supplemental materials of their study [PE19]. We use the open source software XPPAUT [Erm02] to continue a bifurcation in $\mathcal{R}_0$ along the annual attractor for both the stable and unstable branches, and extract the characteristic multipliers associated with these branches. This process is repeated for different forcing functions, including sinusoidal ($p = 1$), square ($p = 0$) and term-time forcing ($p = -1$), along with varying amplitudes of forcing ($\alpha \in \{0, 0.25, 0.5, 0.75, 1\}$). The transient periods of the associated annual attractor for a full range of values of $\mathcal{R}_0$ for these different forms of seasonal forcing and amplitudes of forcing are plotted in fig. 3.2. The other parameter estimates used in constructing these results are given in table 2.1. We plot the period of damped oscillations to the equilibrium of solutions to the unforced SIR model in these figures as well. The damped oscillations associated with the unforced model are computed using eq. (3.14).

The range of transient periods presented in these figures assists in explaining the frequency structure observed in the spectral analysis for the whooping cough mortality time-series carried out in chapter 2. The initial transition analysis we discussed in that chapter only explained the prominent annual pattern observed in the time-series, as the continuation in bifurcations revealed only an annual attractor for reasonable amplitudes of forcing. The transitions to biennial and triennial epidemic cycles across the time-series (see fig. 2.4) may be a result of the transient dynamics and the variation of the effective reproduction number (see section 2.5.3) across the 300-year long time-series.

Although the parameter estimates for whooping cough dynamics yield only an annual attractor for small forcing amplitudes, $\alpha \leq 0.1$, more interesting bifurcations exist for larger amplitudes of forcing. In particular, period-doubling bifurcations in $\mathcal{R}_0$ for $\alpha \geq 0.15$ exist, and it is still possible to obtain the period of damped oscillations onto the annual attractor. It is also possible to compute the period of the oscillations of growing amplitude as the trajectory escapes the annual cycle, which is now a repellor, which is when the period-two orbit arises. We then repeat these numerical computations to find the transient periods onto the stable and unstable branches of the annual cycle for parameter estimates of measles, for which period-doubling bifurcations in $\mathcal{R}_0$ exist for forcing amplitudes as small as 0.08 [HE15]. These results are displayed in fig. 3.4. The parameter estimates used for whooping cough incidence are identical to the parameters used for measles incidence (see table 2.1) except for the mean generation interval. The mean generation interval, which is used as the mean infectious period in the SIR model we use (see section 2.5.1), is 22 days for Whooping Cough [AM91] and 13 days for Measles [AM91].

For small $\mathcal{R}_0$ values, the periods of damped oscillations onto the stable annual attractor are close to the periods of damped oscillations onto the equilibrium of the solution to the unforced model. As $\mathcal{R}_0$ increases, the difference between those damped oscillations increases for all amplitudes of forcing. In fig. 3.2 and fig. 3.4, the period of the damped oscillations of the seasonally forced model approach the value 2 once the attractor reaches a bifurcation point (a period-doubling bifurcation point) and becomes unstable. Note that the dominant characteristic multiplier, λ_k, encodes information about the stability of the associated attractor; if $|\lambda_k| < 1$, the attractor is linearly stable [Str18]. Incidentally, as the period-doubling bifurcation point is approached – where the period-one orbit becomes unstable and the modulus

of the characteristic multiplier exceeds one – the argument of the dominant characteristic multiplier approaches π (i.e., the imaginary component of the associated characteristic multiplier is approaching zero as the trajectories are no longer approaching this branch). This results in the growing oscillations away from the repellor having a period of 2 years (see eq. (3.15)). Note, though, that regions along the stable branch, and near the repellor, have an associated characteristic multiplier with an imaginary component approaching zero. This results in a transient period of 2 years of the associated stable branch of the annual attractor in the approach to the unstable branch.

The exponential rates of decay, r, of these damped oscillations onto the annual attractor, or the rates of growth of the *growing* oscillations away from the annual repellor, for both whooping cough and measles are plotted in fig. 3.3 and fig. 3.5, respectively. The exponential rates of decay of damped oscillations approaching the equilibrium of solutions to the unforced model are given by

$$r = |\mathrm{Re}\,(\lambda)\,|, \tag{3.16}$$

where λ is the dominant eigenvalue of the system. The exponential rates of decay of damped oscillations approaching the annual attractor, or the oscillations growing away from the repellor, of the forced model are given by

$$r_1 = |\lambda_1|, \tag{3.17}$$

where λ_1 is the dominant characteristic multiplier of the associated stroboscopic map. Along the annual attractor (the stable branch of the attractor), the rates of decay of the forced model, for all forcing functions (term-time forcing ($p = -1$), square forcing ($p = 0$) and sinusoidal forcing ($p = 1$)) and amplitudes of forcing ($\alpha \in \{0.25, 0.5, 0.75, 1\}$) considered, match that of the exponential rate of decay of damped oscillations associated with the unforced model. In other words, the rate at which damped oscillatory solutions to the unforced model approach the equilibrium is the same rate as the damped oscillatory solutions to the forced model, regardless of forcing function, approach the stable annual limit cycle. However, this equality breaks when the model approaches the unstable branch of the attractor (the repellor). As a result of the stability of the branch changing, the damped oscillations onto the limit cycle vanish before growing away from the now-unstable branch. This is reflected in fig. 3.3 and fig. 3.5 as the curves of the decay

rates hit the horizontal axis (i.e., $r = 0$) and the period-doubling bifurcation point is marked with a circular point that not-so-coincidentally happens to be at $r = 0$. A similar pattern is observed for the "rebirth" of the stable annual cycle, in which the growing oscillations away from the repellor approach $r = 0$ as the branch becomes stable. This is marked in fig. 3.5 with a square point.

For term-time forcing, this behaviour is not observed for all amplitudes of forcing; we assume this is a result of the lack of fine-resolution in the time-step used to numerically produce these figures. Reconstructing these results using a refined time-step would need to be done to validate this assumption, however. For forcing functions and amplitudes for which only an annual attractor exists for relevant ranges of $\mathcal{R}_0$ (term-time forcing, $p = -1$, with forcing amplitude $\alpha = 0.25$ for whooping cough), we observe the transient period asymptote at $T_1 = 2$ (see fig. 3.2). We also observe the rate at which those oscillations decay onto the annual attractor asymptote slightly about zero and stray from the exponential rate of decay of damped oscillations from the unforced model, which is reflected in the last panel of fig. 3.3. The rates of decay, or rates of growth, influence the magnitude of the associated spectral peak. The quantification of how attractive the associated attractor is, or how repulsive the repellor is, may help to facilitate prediction of the magnitudes of spectral peaks in epidemic time series [BE03].

Studying the transient periods additionally provides an alternative method from methods used by Papst & Earn [PE19] in identifying key bifurcations in $\mathcal{R}_0$. Papst & Earn identified period-doubling bifurcation points by constructing bifurcation diagrams, whereas this result allows us to identify the same period-doubling bifurcations in $\mathcal{R}_0$ along the period-one branch with the associated transient period. Papst & Earn showed this period doubling bifurcation is invariant to the shape of seasonal forcing if the amplitude of forcing is appropriately adjusted. This leads us to ask if the transient decay observed in the seasonally forced SIR model is invariant to the shape of seasonal forcing with an appropriately adjusted amplitude of forcing. The general consistency of the shape of curves in fig. 3.2 and fig. 3.4 additionally suggests there may be invariance in the curves between forcing functions may exist with an appropriately chosen amplitudes of forcing. We explore this invariance in the following section.

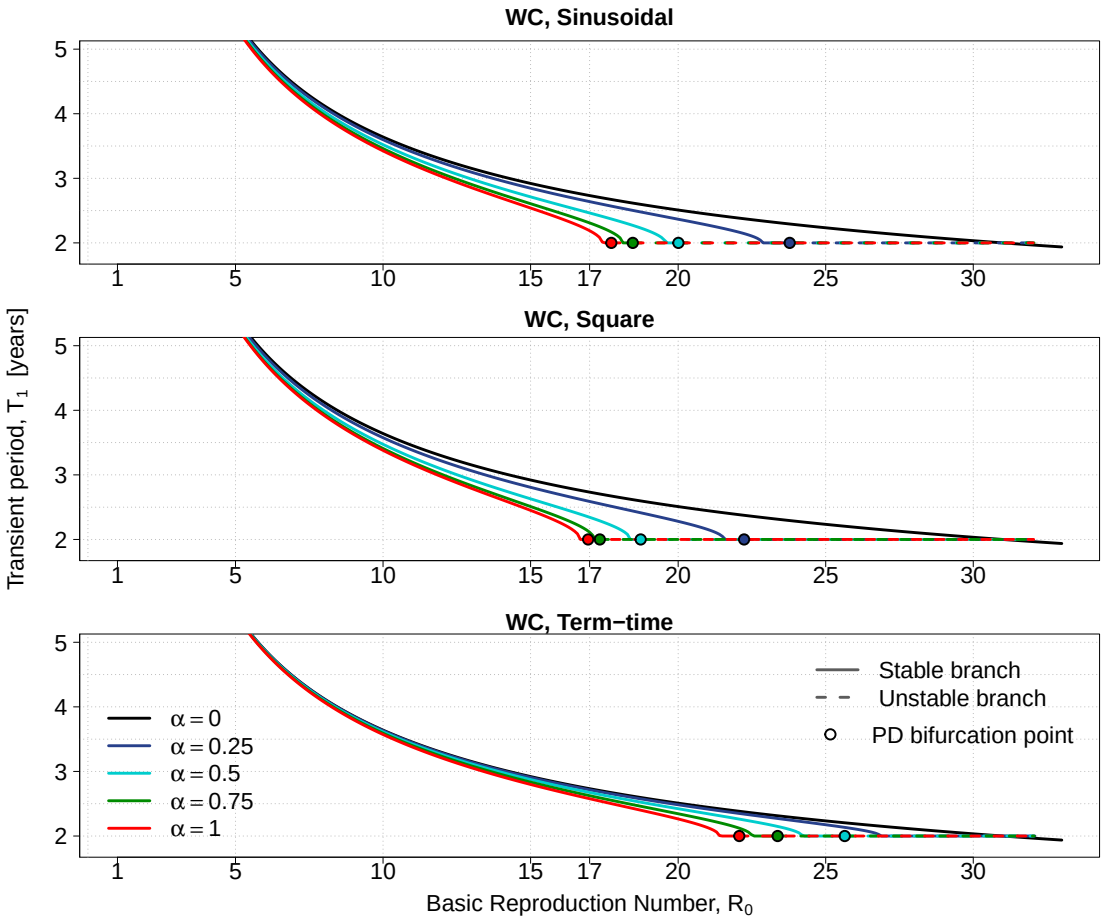

Figure 3.2: Transient periods of the associated *stable and unstable* branches of the annual cycle of the seasonally forced SIR model. The periods are calculated using a mean generation time ($1/\gamma$) of 22 days [AM91], reflecting the mean generation interval of whooping cough. The basic reproduction number of whooping cough, $\mathcal{R}_0 = 17$, estimated in 1950 by Anderson and May [AM91], is labeled along the horizontal axis. The periods of the damped oscillations derived from the unforced SIR model are plotted in each panel in black (i.e., $\alpha = 0$). The period of damped oscillations onto the annual attractor for forcing amplitudes $\alpha \in \{0.25, 0.5, 0.75, 1\}$ are color coded in each panel, where each panel are given forcing functions (term-time forcing ($p = -1$), square forcing ($p = 0$) and sinusoidal forcing ($p = 1$)). The solid lines refer to the transient periods of the associated stable branches of the annual attractor, while the dashed lines refer to the transient periods of the associated unstable branches of the annual attractor, or repellor. The period-doubling bifurcation point is marked with a circular point. Note that in the last panel, for term-time forcing ($p = -1$), the curve for the amplitude of forcing $\alpha = 0.25$ is stable throughout the entire range of $\mathcal{R}_0$ values presented, however, the lines collated on top of one another make this distinction difficult to see.

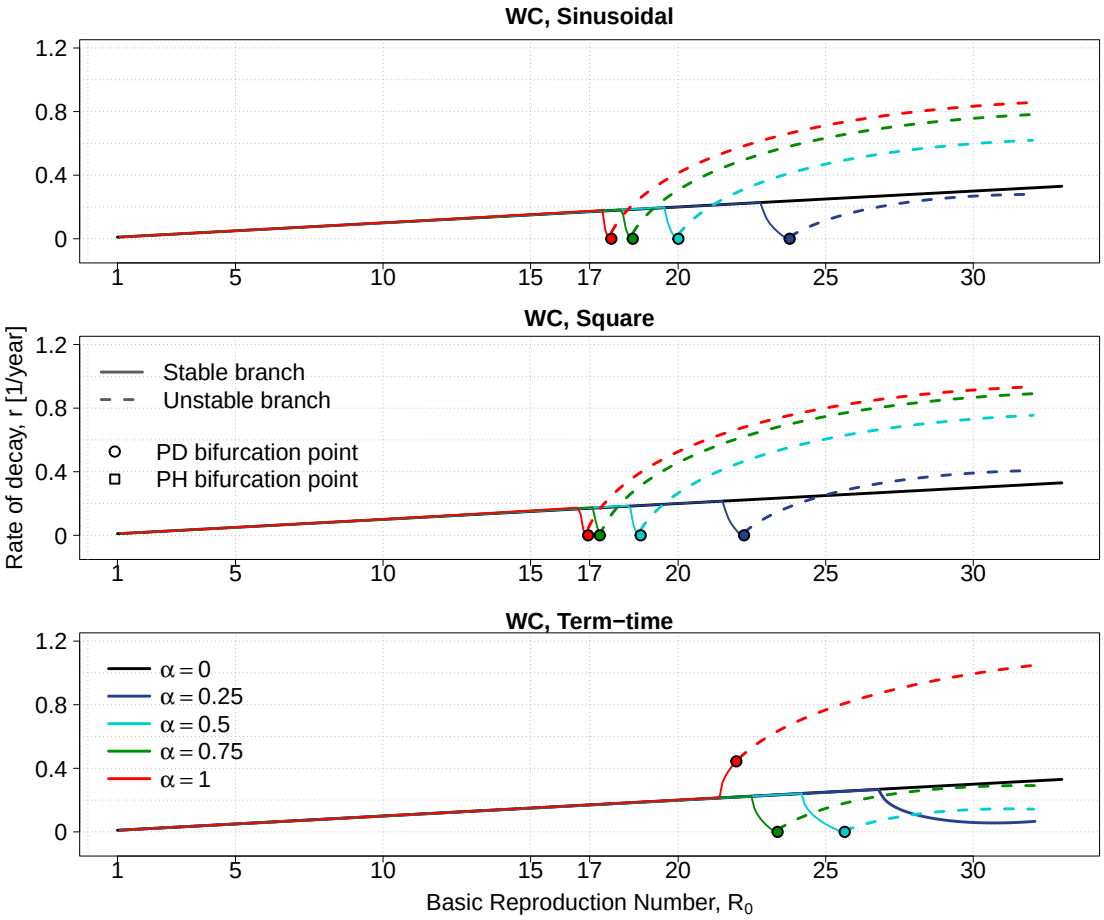

Figure 3.3: Exponential rate of decay of the oscillations onto the annual attractor, or away from the annual repellor, of the seasonally forced SIR model. The periods are calculated using a mean generation time ($1/\gamma$) of 22 days [AM91], reflecting the mean generation interval of whooping cough. The basic reproduction number of whooping cough, $\mathcal{R}_0 = 17$, estimated in 1950 by Anderson and May [AM91], is labeled along the horizontal axis. The rates of decay of the damped oscillations derived from the unforced SIR model are plotted in each panel in black (i.e., $\alpha = 0$). The decay rates of damped oscillations onto the annual attractor for forcing amplitudes $\alpha \in \{0.25, 0.5, 0.75, 1\}$ are color coded in each panel, where each panel are given forcing functions (term-time forcing ($p = -1$), square forcing ($p = 0$) and sinusoidal forcing ($p = 1$)). The solid lines refer to the rates of decay of oscillations approaching the associated stable branches of the annual attractor, while the dashed lines refer to the rates of decay of oscillations growing away from the annual repellor. The period-doubling bifurcation point is marked with a circular point.

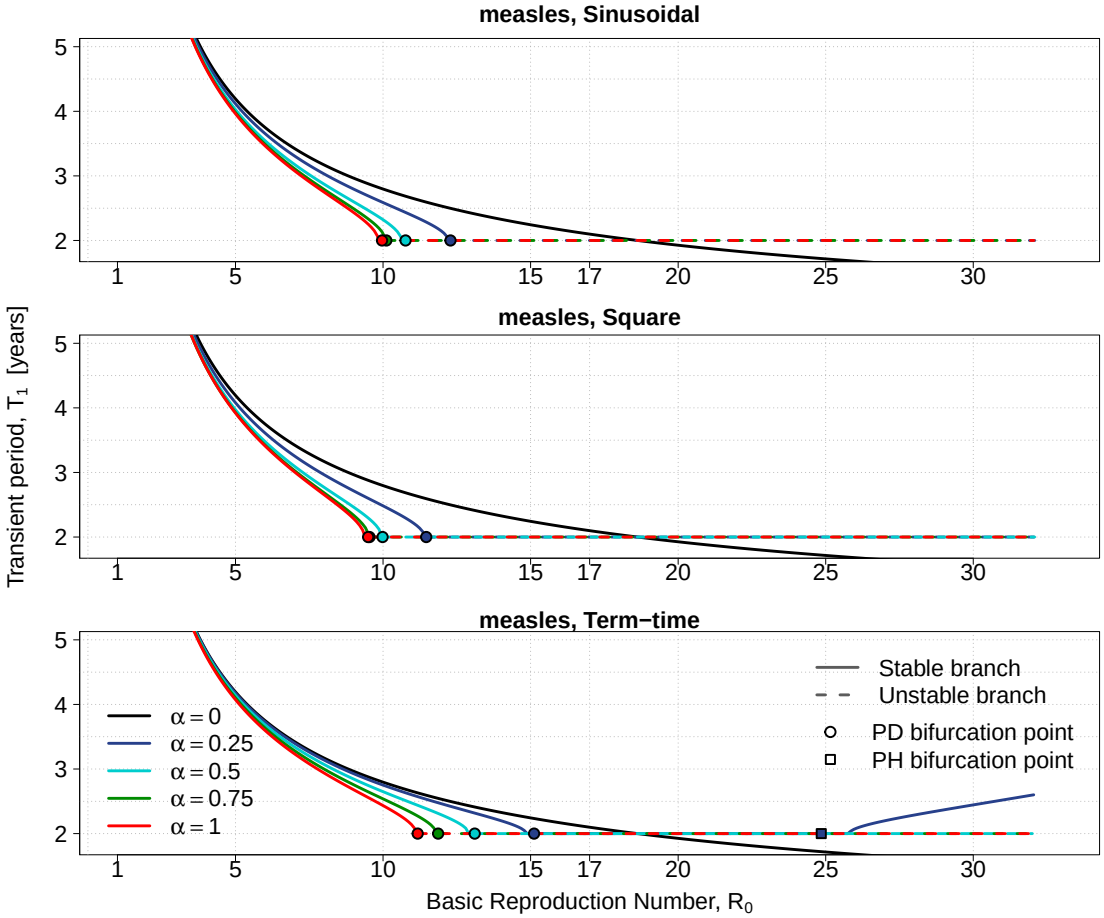

Figure 3.4: Transient periods of the associated *stable and unstable* branches of the annual cycle of the seasonally forced SIR model. The periods are calculated using a mean generation time ($1/\gamma$) of 13 days [AM91], reflecting the mean generation interval of measles. The basic reproduction number of measles, $\mathcal{R}_0 = 17$, estimated in 1950 by Anderson and May [AM91], is labeled along the horizontal axis. The style of this figure is identical to that of fig. 3.2, except it is computed for measles. The period-halving bifurcation point (or reverse fold bifurcation point), is marked with a square point.

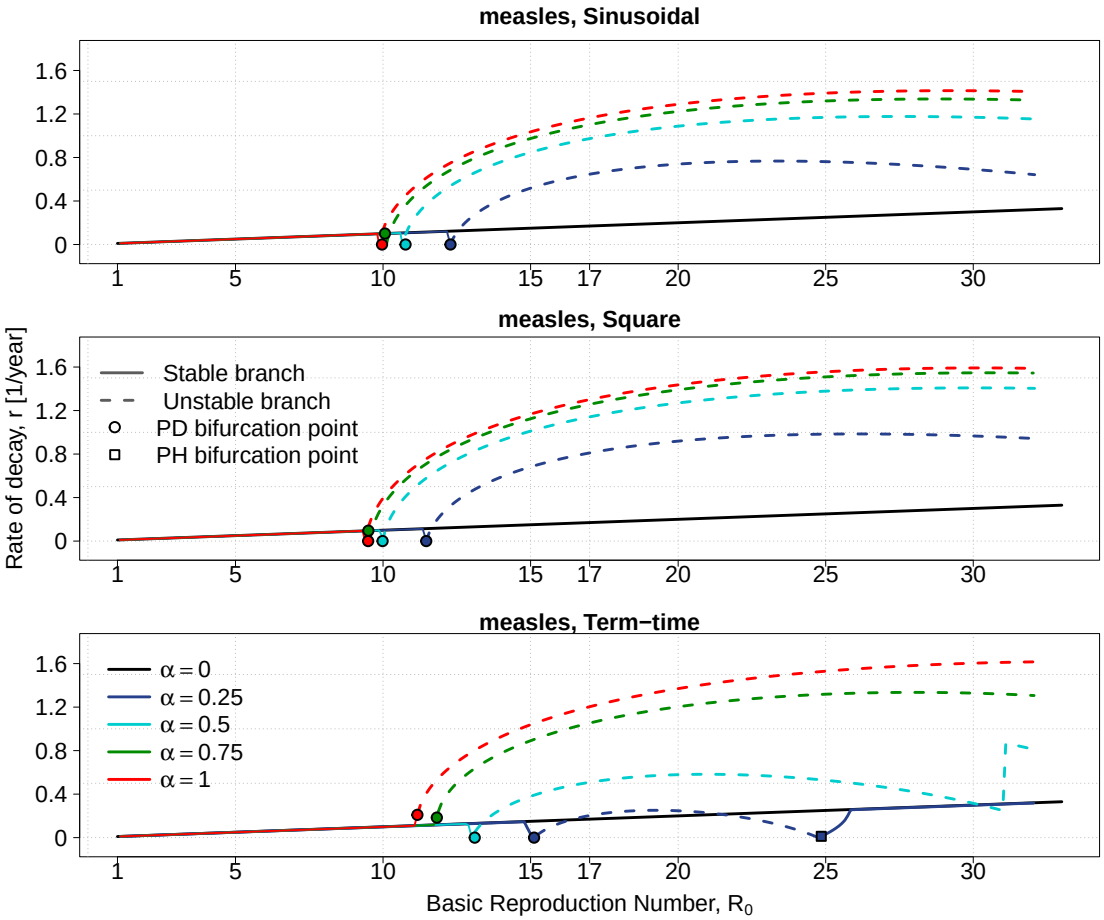

Figure 3.5: Exponential rate of decay of the oscillations onto the annual attractor, or away from the annual repellor, of the seasonally forced SIR model. The periods are calculated using a mean generation time $(1/\gamma)$ of 13 days [AM91], reflecting the mean generation interval of measles. The basic reproduction number of measles, $\mathcal{R}_0 = 17$, estimated in 1950 by Anderson and May [AM91], is labeled along the horizontal axis. The style of this figure is identical to that of fig. 3.3, except it is computed for measles. The period-halving bifurcation point (or reverse fold bifurcation point), is marked with a square point.

3.5 Invariance in the transient decay resulting under radically different forms of seasonal forcing

We begin exploring the potential invariance in the periods of damped oscillations onto the annual attractor from different seasonal patterns by considering the invariant sets of parameters Papst & Earn discovered for measles incidence. The invariant sets of parameters refers to sets containing the parameter pairs $\left\{ \left(p_0, \alpha_0\right), \left(p_1, \alpha_1\right), \ldots, \left(p_i, \alpha_i\right) \right\}$, where p_i is a given shape parameter from the family of forcing functions (see Section 3.2) and α_i is an amplitude of forcing such that all parameter pairs in the set yield the same key bifurcations in $\mathcal{R}_0$. The invariant set of parameters Papst & Earn found lead to invariance in the key bifurcations are detailed in table 3.1. This table is directly from Papst & Earn's work, and outlines the quantitative invariance in fold bifurcations. By matching where the principal period-doubling bifurcation in $\mathcal{R}_0$ occurs using bifurcation diagrams in $\mathcal{R}_0$ for invariant (p, α) pairs, Papst & Earn found invariance in fold bifurcations that give rise to a period n attractor, ranging from period 3 attractors to period 7 attractors. From these invariant parameter sets, we replicate fig. 3.4 for $p = -1$ (term-time forcing), $p = 0$ (square forcing) and $p = -1$ (sinusoidal forcing) with the appropriate forcing amplitude from table 3.1. These results can be seen in fig. 3.6 and fig. 3.4. We additionally recreate table 3.1 with the numerical results from our analysis in fig. 3.6. This figure displays the equality of the transient periods onto the stable branch of the annual attractor before the principal period-doubling bifurcation is reached, which occurs near $\mathcal{R}_0 = 15.12$. However, the same invariance does not exist for the death of the period-two attractor, or the "rebirth" of the annual attractor. This aligns with the lack of invariance that Papst & Earn found for the death of these period-two orbits, "Thus, the observed quantitative invariance is restricted to the 'births' of these branches and not their 'deaths'." [PE19]. Regardless, the invariance in the transient decay onto the annual attractor prior to the 'birth' of the period-two attractor exists and is numerically validated in table 3.2.

This invariance in the transient periods likely exists for attractors of higher periods. In particular, we predict these results of invariance can be reproduced for the fold bifurcations of periods three up through seven that are detailed in table 3.1. For example, we predict the possibility the transient periods of the

associated period-two attractor may display invariance for the invariant parameter sets considered in this section up until the the fold-3 bifurcation point is reached. Further work needs to be done to validate the possibility of the invariance in the transient periods of associated attractors of higher periods. Additionally, only invariance for measles has been demonstrated. We expect there exists an invariant parameter set similar to that of measles for whooping cough that would result in the same invariance of transient periods of the associated annual attractor and attractors of higher periods. Again, however, further work needs to be done to validate this assumption.

More importantly, the results from this chapter, namely the invariance of the transient decay of the associated annual attractor from different forms of seasonal forcing, provide an alternative method to study the transitions of epidemics. For diseases such as whooping cough that exhibit only an annual attractor for relevant $\mathcal{R}_0$ values and reasonable amplitudes of forcing, we have shown that with an appropriately adjusted amplitude of forcing, the transient dynamics are invariant to the shape of seasonal forcing. This allows the use of the more convenient *sinusoidally* forced SIR model to be used when analyzing the transient dynamics of diseases like whooping cough. More importantly, the invariance in the transient periods means we can compare temporal epochs from observed mortality (or incidence) data when both the amplitude of forcing and the shape of forcing are different by transforming the shape of one to be identical with the other. We have additionally shown the invariance in the transient periods from different forms of seasonal forcing exists along the stable branch of the annual attractor for diseases that do have period-doubling bifurcations in $\mathcal{R}_0$ for relevant amplitudes of forcing, such as measles. Rather than constructing one-parameter bifurcation diagrams in $\mathcal{R}_0$ for various amplitudes of forcing and matching these diagrams with similar diagrams constructed with observed seasonal patterns in order to estimate the amplitude of forcing (the method of transition analysis used in previous works [KE20, HE15, PE19]), the transient periods onto the annual attractor can be matched instead. Furthermore, this provides a method for estimating the forcing amplitude of the sinusoidally forced model for whooping cough. Although this method of estimation is not carried out in this thesis, we aim to complete this goal in future work.

Forcing parameters		$\mathcal{R}_0$ **bifurcation point**					
p	α	**PD (2)**	**fold (3)**	**fold (4)**	**fold (5)**	**fold (6)**	**fold (7)**
−1.00	0.2500	15.1199	8.8991	6.2374	4.9755	4.2623	3.8094
−0.50	0.1012	15.1254	8.9014	6.2363	4.9713	4.2554	3.7995
0.00	0.0782	15.1146	8.8946	6.2247	4.9554	4.2357	3.7758
0.25	0.0839	15.1248	8.8992	6.2292	4.9599	4.2401	3.7800
1.00	0.1000	15.1234	8.8976	6.2269	4.9571	4.2370	3.7767
2.00	0.1182	15.1240	8.8972	6.2261	4.9558	4.2354	3.7749
Relative Difference		**0.0004**	**0.0005**	**0.0020**	**0.0040**	**0.0063**	**0.0090**

Table 3.1: Invariance of fold bifurcations at different $\mathcal{R}_0$ values when the principal period doubling (PD) bifurcation at $\mathcal{R}_0 = 15.12$ is matched. This table is taken directly from Papst & Earn ([PE19], Table 1). Fold (n) refers to a fold bifurcation that gives rise to a period n attractor as $\mathcal{R}_0$ is increased. The relative difference is computed by taking the maximum of $\left(x - x_{tt}\right)/x_{tt}$, where x is the value of $\mathcal{R}_0$ at the bifurcation of interest and x_{tt} is its value for term-time forcing ($p = -1$). This table included for comparison with our results in table 3.2, specifically for the relative difference between the period-doubling bifurcation points.

Forcing parameters		$\mathcal{R}_0$ **bifurcation point**	
p	α	**PD (2)**	**PH (1)**
−1.00	0.2500	15.1178	24.8496
0.00	0.0782	15.1131	25.2932
1.00	0.1000	15.1214	25.2319
Relative Difference		**0.0003**	**0.0179**

Table 3.2: Variance of reserve fold bifurcations at different $\mathcal{R}_0$ values when the principal period-doubling bifurcation (PD) at $\mathcal{R}_0 = 15.12$ is matched. Computed for measles. This table is recreated from Papst & Earn ([PE19], Table 1) using the method described in this chapter (the process of matching the period-doubling bifurcation point by examining invariance of the transient periods of the associated annual attractor). "PD" refers to the period-doubling bifurcation point in $\mathcal{R}_0$, while "PH" refers to the period-halving, or the death of the period-two orbit and rebirth of the period-one orbit, which we call a reverse fold bifurcation in $\mathcal{R}_0$. The relative difference is computed by taking the maximum of $\left(x - x_{tt}\right)/x_{tt}$, where x is the value of $\mathcal{R}_0$ at the bifurcation of interest and x_{tt} is its value for term-time forcing ($p = -1$). The relative difference between the period-doubling bifurcation points from our results are similar to those of Papst & Earn, and can be seen in the relative difference for the period-doubling bifurcation points in table 3.1. This further validates the invariance of the transient periods of the associated annual attractor up until the period-doubling bifurcation in $\mathcal{R}_0$ seen in fig. 3.6

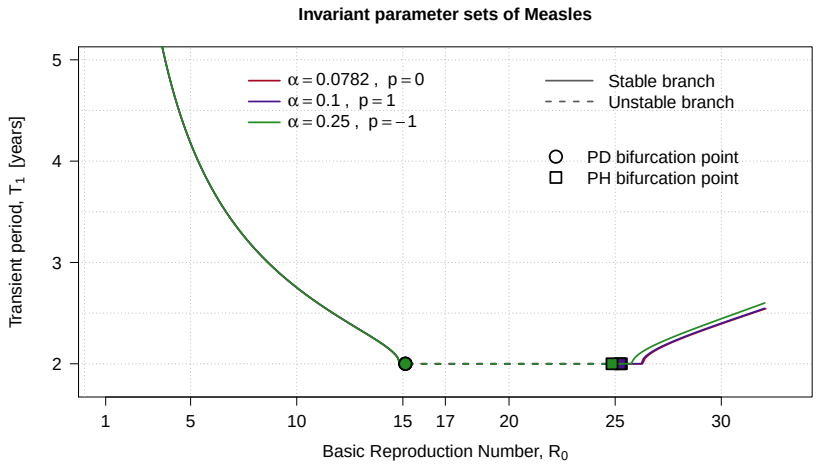

Figure 3.6: Transient periods of the associated *stable and unstable* branches of the annual cycle of the SIR model using the invariant parameter sets from Papst & Earn [PE19]. The periods are calculated using a mean generation time ($1/\gamma$) of 13 days [AM91], reflecting the transient dynamics of measles. The basic reproduction number of measles, $\mathcal{R}_0 = 17$, estimated in 1950 by Anderson and May [AM91], is labeled along the horizontal axis. The solid lines refer to the transient periods of the associated stable branches of the annual attractor, while the dashed lines refer to the transient periods of the associated unstable branches of the annual attractor, or repellor. The curves of the transient periods are color coded according to which (p, α) pair is being plotted. The period-doubling bifurcation point is marked with a circular point, while the period-halving bifurcation point (or reverse fold bifurcation point), is marked with a square point. The (p, α) pairs for which the transient periods are plotted are as follows: $(p = 0, \alpha = 0.0782)$, $(p = 1, \alpha = 0.1000)$, and $(p = -1, \alpha = 0.2500)$. Note the overlap of the transient periods between all three (p, α) pairs prior to the period-doubling bifurcation point at $\mathcal{R}_0 \approx 15.12$ (labeled "PD Bifurcation point"), creating the illusion only the transient periods for the pair $(p = -1, \alpha = 0.2500)$ is being plotted. Furthermore, we have validated the invariance of the transient periods of the associated annual attractor up until the period-doubling bifurcation point from radically different forms of seasonal forcing with appropriately adjusted amplitudes of forcing, where Papst & Earn first discovered this invariance in fold bifurcations.

Chapter 4

Discussion

This thesis began by analyzing whooping cough dynamics in London from 1664-1950. We used a historical whooping cough mortality time-series collected from meticulously kept sources, LBoM [Cre94] and RGWRs [RGW], in which a spectral analysis of the time-series revealed annual, biennial, triennial and even quadrennial epidemic, or inter-epidemic, cycles. We originally sought to model and explain these transitions in the frequency structure of the whooping cough mortality data using the sinusoidally forced SIR model. The method of transition analysis previously used on historical disease-induced mortality time-series, including measles and smallpox [HE15, KE13, Kry11], relies on the existence of a period-doubling bifurcation in $\mathcal{R}_0$ in relevant values of $\mathcal{R}_0$ and reasonable amplitudes of forcing, α. Our analysis using this method on whooping cough, however, revealed the existence of only an annual attractor for relevant values of $\mathcal{R}_0$ and amplitudes of forcing. Furthermore, we were unable to apply this method of transition analysis to explain the the transitions in the frequency structure observed in the whooping cough mortality time-series. The lack of bifurcations in relevant parameter spaces of our model for whooping cough led us to investigate the transient dynamics instead. Conveniently, the transient periods of the associated annual attractor have the potential to explain the transitions seen in the frequency structure of whooping cough mortality. The analysis in chapter 3, particularly the results presented in fig. 3.2, show transient periods ranging from five years to two years along the ranges of estimates for the effective reproduction number of whooping cough (see table 2.1).

We additionally considered a family of forcing functions when analyzing the transient dynamics (see section 3.2) as prior to this work, it was unknown if the transient dynamics of the seasonally forced SIR model were invariant to the shape of seasonal forcing. Papst & Earn showed that key bifurcations, namely fold bifurcations, of the standard SIR model are invariant to the shape of seasonal forcing if the amplitude of forcing is appropriately adjusted [PE19]. This finding reinforced the method of transition analysis, in

which period-doubling bifurcations in $\mathcal{R}_0$ of the sinusoidally forced SIR model are matched with period-doubling bifurcations in $\mathcal{R}_0$ of the SIR model forced with observed seasonal patterns in order to estimate the forcing amplitude. Our results from chapter 3 expand upon Papst & Earn's findings. We discovered invariance in the decay of transient periods of the associated annual attractor from radically different shapes of seasonal forcing with appropriately adjusted amplitudes of forcing.

This result suggests an alternative method of transition analysis and estimation of the forcing amplitude for the sinusoidally forced SIR model. Rather than matching period-doubling bifurcation points of the sinusoidally forced model and the model forced with the observed seasonal patterns to estimate the forcing amplitude, transient periods of the associated annual attractor, up until the period-doubling bifurcation in $\mathcal{R}_0$, can be matched between these two differently forced models. We aim to complete this work in modelling and analyzing whooping cough dynamics in London from 1664-1950 in the future.

While the main result from chapter 3 provides an alternative method of transition analysis, it still does not explain the underlying cause of invariant dynamics for different forms of seasonal forcing. Papst & Earn built upon work from Bauch et al. [BE03] in trying to understand this resulting invariance. Bauch et al. had suggested fixing the average spectral power in forcing functions could potentially conserve bifurcation structure. However, Papst & Earn did further work in this direction and found that fixing the average spectral power in the forcing function does not conserve bifurcation structure [PE19]. In regards to the resulting invariance of transient dynamics, further work needs to be done to verify the invariance, or lack of invariance, of transient dynamics associated with higher-period attractors. Papst & Earn demonstrated the resulting invariance of fold bifurcations up to periods of 7, while we only verified invariance of transient dynamics up to the period-doubling bifurcation in $\mathcal{R}_0$. We also did not consider the full range of family of forcing functions that Papst & Earn considered, and further research can be done in validating the resulting invariance of the decay of the transient periods.

Another avenue of future work arising from the results in chapter 3 is the possibility of finding an analytical expression for the transient periods of the associated annual attractor in terms of the amplitude of forcing, α, and $\mathcal{R}_0$. We have an analytical expression in terms of the model parameters for the period of damped oscillations onto the equilibrium of solutions to the unforced model (see the black curves in fig. 3.2

and fig. 3.4). The transient periods of the associated annual attractor follow this curve from the unforced model closely for small $\mathcal{R}_0$. The curves of the transient periods have a turning point as $\mathcal{R}_0$ increases that looks similar to arctan or a sigmoidal-like factor being applied to the unforced analytical expression where the inputs are α and $\mathcal{R}_0$. Furthermore, finding an analytical expression for these curves would provide a seamless method for estimating the amplitude of forcing for the sinusoidally forced model, and such an analytical expression could potentially lend insight into the underlying cause of this resulting invariance. While one could use curve-fitting methods to approximate the curves of the transient periods, the insight, and convenience, that would follow from analytically deriving such an expression would be valuable. He & Earn examined the variational equations of the seasonally forced SIR model [HE07]. Following such derivations may be a starting point for such a pursuit.

In conclusion, the method of transition analysis introduced by Earn et al. [ERBG00], which has been used in the study of historical infectious disease dynamics [KE13, Kry11, HE15], is a powerful tool for understanding and predicting changes in infectious disease dynamics. While we have not yet been able to apply this method to try to explain the multi-year period epidemic cycles observed in the whooping cough mortality time-series in historical London, it still provided insights into the dynamics of whooping cough that motivated the investigation of the transient dynamics. The investigation of the transient dynamics led to the main result of this thesis; the invariance of transient decay from different forms of seasonal forcing. While future work on understanding and validating this invariance needs to be completed, we now have a method for modelling and analyzing diseases such as whooping cough that exhibit only annual resonant epidemic periods.

Bibliography

[AM91] Roy M Anderson and Robert M May, *Infectious Diseases of Humans: Dynamics and Control*, Oxford University Press, May 1991.

[AML24] Christopher P. Zabbo. Ashley M. Lauria, *Pertussis*, StatPearls, StatPearls Publishing, 2024.

[Arc] ArcGIS, *London historical boundaries - overview*.

[BE03] Chris T. Bauch and David J. D. Earn, *Transients and attractors in epidemics*, Proceedings of the Royal Society of London. Series B: Biological Sciences **270** (2003), 1573–1578.

[Can14] Public Health Agency of Canada, *Pertussis (whooping cough): For health professionals*, January 2014, Last Modified: 2024-03-07.

[Cre94] Charles Creighton, *A History of Epidemics in Britain, Volume 2; From the Extinction of Plague to the Present Time*, 1894, p. 671.

[Dat15] London Datastore, *Historical census tables*, 2015.

[DC96] Scott S. Duncan CJ, Duncan SR, *Whooping cough epidemics in London, 1701-1812: infection dynamics, seasonal forcing and the effects of malnutrition*, Proc Biol Sci. (1996).

[Dep13] Statistica Research Department, *Number of live births in the United Kingdom (U.K.) from 1900 to 1930*, 2013.

[Ear09] D. J. D Earn, *Mathematical epidemiology of infectious diseases*, Mathematical Biology (M. A. Lewis, M. A. J. Chaplain, J. P. Keener, and P. K. Maini, eds.), IAS/Park City Mathematics Series, vol. 14, American Mathematical Society, 2009, pp. 151–186.

[ERBG00] David J. D. Earn, Pejman Rohani, Benjamin M. Bolker, and Bryan T. Grenfell, *A Simple Model for Complex Dynamical Transitions in Epidemics*, Science **287** (2000), 667–670.

[Erm02] Bard Ermentrout, *Simulating, analyzing, and animating dynamical systems: a guide to xppaut for researchers and students. software, environments, and tools.*, Philadelphia, PA: Society for Industrial and Applied Mathematics, 2002.

[HE07] Daihai He and David J.D. Earn, *Epidemiological effects of seasonal oscillations in birth rates*, Theoretical Population Biology **72** (2007), 274–291.

[HE15] Karsten Hempel and David J. D. Earn, *A century of transitions in New York City's measles dynamics*, Journal of The Royal Society Interface **12** (2015), no. 106.

[Het76] Herbert W. Hethcote, *Qualitative analyses of communicable disease models*, Mathematical Biosciences **28** (1976), no. 3, 335–356.

[KE13] Olga Krylova and David J. D. Earn, *Effects of the infectious period distribution on predicted transitions in childhood disease dynamics*, Journal of The Royal Society Interface **10** (2013), Publisher: Royal Society.

[KE20] Olga Krylova and David J. D. Earn, *Patterns of smallpox mortality in London, England, over three centuries*, PLOS Biology **18** (2020).

[KM91] W. O. Kermack and A. G. McKendrick, *Contributions to the mathematical theory of epidemics–I. 1927*, Bulletin of Mathematical Biology **53** (1991), 33–55.

[KO09] Donghoh Kim and Hee-Seok Oh, *EMD: A Package for Empirical Mode Decomposition and Hilbert Spectrum*, The R Journal **1** (2009).

[Kry11] Olga Krylova, *Predicting epidemiological transitions in infectious diseas dynamics: smallpox history in London (1664-1930)*, Ph.D. thesis, McMaster University, 2011.

[LY73] Wayne P. London and James A. Yorke, *Recurrent outbreaks of measles, chickenpox and mumps: I. seasonal variantion in contact rates*, American Journal of Epidemiology **98** (1973), no. 6, 453–468.

[MD86] M. J. Murphy and T. P. G. Dyson, *Vital Statistics Time Series, 1749-1982*, 1986, Version Number: 1st Edition.

[oS] PennState Eberly College of Science, *12. Spectral Analysis – STAT 510 | Applied Time Series Analysis*.

[PE19] Irena Papst and David J. D. Earn, *Invariant predictions of epidemic patterns from radically different forms of seasonal forcing*, Journal of The Royal Society Interface **16** (2019).

[PE24] Todd L. Parsons and David J. D. Earn, *Uniform asymptotic approximations for the phase plane trajectories of the sir model with vital dynamics*, SIAM Journal on Applied Mathematics **84** (2024), no. 4, 1580–1608.

[Pyk19] Jordan Pyke, *Transitions in London measles dynamics*, Master's thesis, McMaster Univserity, 2019.

[R C24] R Core Team, *R: A language and environment for statistical computing*, R Foundation for Statistical Computing, Vienna, Austria, 2024.

[RGW] *Weekly return of births and deaths in London / published by authority of the Registrar-General.*

[RS18] Angi Roesch and Harald Schmidbauer, *Waveletcomp: Computational wavelet analysis*, 2018, R package version 1.1.

[Sch84] Dieter Schenzle, *An Age-Structured Model of Pre- and Post-Vaccination Measles Transmission*, IMA Journal of Mathematics Applied in Medicine & Biology **1** (1984), no. 2, 169–191.

[Str18] Steven Strogatz, *Nonlinear dynamics and chaos : with applications to physics, biology, chemistry, and engineering*, Second edition. Boulder, CO : Westview Press, 2018.

[TC98] Christopher Torrence and Gilbert P. Compo, *A Practical Guide to Wavelet Analysis*, Bulletin of the American Meteorological Society **79** (1998), no. 1, 61–78.

[U.K] Health Security Agency of U.K., *Confirmed cases of pertussis in England by month*.

[Wes12] Robert Weston, *Whooping Cough: A Brief History to the 19th Century*, Canadian Bulletin of Medical History = Bulletin Canadien D'histoire De La Medecine **29** (2012), 329–349.

[WHO18] *Pertussis: Vaccine Preventable Diseases Surveillance Standards*, 2018.